2019

Type 2 Diabetes Leads to Impairment of Cognitive Flexibility and Disruption of Excitable Axonal Domains in the Brain

Leonid M. Yermakov
Wright State University

TYPE 2 DIABETES LEADS TO IMPAIRMENT OF COGNITIVE FLEXIBILITY AND DISRUPTION OF EXCITABLE AXONAL DOMAINS IN THE BRAIN

A dissertation submitted in partial fulfillment of the
requirements for the degree of
Doctor of Philosophy

by

LEONID M. YERMAKOV
B.S., Emory University, 2014

2019
Wright State University

WRIGHT STATE UNIVERSITY

GRADUATE SCHOOL

March 1, 2019

I HEREBY RECOMMEND THAT THE DISSERTATION PREPARED UNDER MY SUPERVISION BY Leonid M. Yermakov ENTITLED Type 2 Diabetes Leads to Impairment of Cognitive Flexibility and Disruption of Excitable Axonal Domains in the Brain BE ACCEPTED IN PARTIAL FULFILLMENT OF THE REQUIREMENTS FOR THE DEGREE OF Doctor of Philosophy.

_____
Keiichiro Susuki, M.D., Ph.D.
Dissertation Director

_____
Mill W. Miller, Ph.D.
Director, Biomedical Sciences Ph.D. Program

_____
Barry Milligan, Ph.D.
Interim Dean of the Graduate School

Committee on Final Examination:

_____
Keiichiro Susuki, M.D., Ph.D.

_____
Mark M. Rich, M.D., Ph.D.

_____
Kathrin L. Engisch, Ph.D.

_____
Khalid M. Elased, Pharm.D., Ph.D.

_____
Lynn K. Hartzler, Ph.D.

ABSTRACT

Yermakov Leonid M. Ph.D., Biomedical Sciences Ph.D. Program, Wright State University, 2019. Type 2 Diabetes Leads to Impairment of Cognitive Flexibility and Disruption of Excitable Axonal Domains in the Brain.

Type 2 diabetes is a metabolic disease affecting millions of people around the world. Cognitive and mood impairments are among its many debilitating complications, but disease mechanism(s) remain elusive. Here, we present a series of behavioral tasks that demonstrate impairment of cognitive flexibility in *db/db* mice, a commonly used type 2 diabetes model. Using immunohistochemistry, we demonstrate disruption of axon initial segments (AIS) and nodes of Ranvier, excitable axonal domains regulating neuronal output, in brain regions associated with cognitive and mood impairments. Finally, we present results of exercise treatment that ameliorates AIS disruption in these animals. Establishing cognitive flexibility deficits in *db/db* mice that parallel disease complications in patients with type 2 diabetes allows future research to test novel treatment strategies, while discovering disruption of excitable axonal domains fills the missing gap in our understanding of disease pathophysiology.

TABLE OF CONTENTS

LIST OF FIGURES

ACKNOWLEDGMENTS

I would like to thank the Wright State University Boonshoft School of Medicine and the Graduate School, specifically the Biomedical Sciences Ph.D. program, for giving me this unique opportunity.

I would like to thank my incredible mentor Dr. Keiichiro Susuki. You have been kind, supportive, and patient with me over these years. I will never forget the day when I came to your office and you showed me the beautiful and mysterious nodes of Ranvier under the microscope for the first time. I will also always remember and cherish your adept guidance and endless encouragement throughout my Ph.D. journey—I could never wish for a more perfect mentor during these challenging years!

I would also like to thank all the current and previous lab members of the Susuki Lab, including Dr. Yoshinori Otani, Dr. Ryan Griggs, Domenica Drouet, Sholeh Bazrafshan, Duc Nguyen, Jeneane Jaber, Andrea Bell, John Miller, Rael Sammeroff and Melinda Meiring for their support and comradery.

I would like to thank the wonderful and extremely supportive LAR staff, who made my life so much more manageable.

I would like to thank my brilliant committee members, who always found time in their busy schedules to come to my talks and provide me with invaluable advice (I promise I will make my slides less busy).

I would like to thank Dr. Charles Vorhees and Dr. Michael Williams, Chiho Sugimoto and Adam Fritz who opened their lab and wholeheartedly supported my project.

I would like to thank all the incredibly supportive professors of Wright State University, who were always willing to teach me new skills and share their knowledge.

I would like to thank my close friends who helped me de-stress and think positively through the difficult times.

Lastly and most importantly, I would like to thank my family: my loving parents and brother, and my wife/best friend/partner in crime Lulu (who was also a Susuki Lab member at one point) for all the courage, love and never-ending support, even despite the thousands of miles that separated us in the end.

Thank you! None of this would have been possible without your support.

PURPOSE AND AIMS

Purpose

Type 2 diabetes prevalence worldwide is growing at an alarming rate. There is an established risk of dementia and depression in patients with type 2 diabetes, as well as a growing awareness of subtle structural and functional cerebral changes that precede development of major neuropsychiatric deficits. One of the key challenges is elucidation of mechanisms behind these brain changes that would allow for creation of disease-modifying treatments and prevention strategies.

The purpose of this research work is two-fold. First, we investigate if leptin-receptor deficient *db/db* mice are suitable for studying impairment of executive functioning, a cognitive domain commonly affected in patients with type 2 diabetes. Second, we examine excitable axonal domains in the brain regions linked to cognitive and mood impairments in type 2 diabetes. Together, these findings will further our understanding of diabetes-associated cognitive dysfunction and provide a model for testing future treatment avenues.

Specific Aims

Specific Aim 1.

Hypothesis: Executive functioning is impaired in type 2 diabetic db/db mice.

Impairment of executive functioning is a major peril for patients with type 2 diabetes, reducing quality of life and ability for diabetes management. Despite the significance of this impairment, the status of executive functions has been largely overlooked in diabetic animal models. Using a battery of behavioral tasks, we evaluate executive functioning in *db/db* mice, a model of type 2 diabetes, during early and prolonged disease stages. We expect to identify impairment in one or more of the executive functions, making *db/db* mice suitable for future testing of this important cognitive domain.

Specific Aim 2.

Hypothesis: Excitable axonal domains are disrupted in brain regions linked to cognitive and mood impairment in type 2 diabetic db/db mice.

Disruption of excitable axonal domains has been identified in several central nervous system diseases, such as multiple sclerosis, schizophrenia and stroke. The implication for this disruption is disturbed neuronal network activity, which, in turn, produces cognitive and mood deficits observed in these diseases. Using immunohistochemistry, we examine excitable axonal domains in the brain regions linked to cognitive and mood impairment in *db/db* mice during early and prolonged disease stages. We expect to identify disruption in the excitable axonal domains in *db/db* mice, providing a novel target for disease-modifying treatments and prevention strategies.

Specific Aim 3.

Hypothesis: Exercise treatment reduces Axon Initial Segment shortening in type 2 diabetic db/db mice.

We observed significant shortening of axon initial segment (AIS), one of the excitable axonal domains, in *db/db* mice starting as early as 10 weeks of age. To determine if AIS shortening was caused by type 2 diabetes, we implement exercise treatment in pre-diabetic 5-week-old *db/db* mice and evaluate AIS length at 10 weeks of age. We expect that glycemic control via exercise significantly reduces the degree of AIS shortening.

BACKGROUND

Type 2 Diabetes and Cognitive Impairment

Cognitive and mood impairments are becoming more frequently recognized as major neuropsychiatric deficits that interfere with daily lives of patients with type 2 diabetes (Wrighten et al., 2009; Thabit et al., 2012; Stoeckel et al., 2016; van Sloten and Schram, 2018).

The risk of dementia is more than doubled in older patients with type 2 diabetes (Stoeckel et al., 2016), but even without dementia, patients with type 2 diabetes experience subtle cognitive deficits across all ages (Biessels et al., 2014). Among cognitive impairments observed in patients with type 2 diabetes are impaired long-term memory (Gold et al., 2007; Palta et al., 2014), cognitive flexibility (Thabit et al., 2012; Sadanand et al., 2016), and working memory (Chen et al., 2014b). Neuroanatomical abnormalities in the prefrontal cortex (Kumar et al., 2008) and hippocampus (Gold et al., 2007)—key brain regions associated with cognition and mood—have been observed using MRI of patients with type 2 diabetes. In addition to its negative impact on quality of life, diabetes-related cognitive dysfunction can exacerbate the course of the disease, since treatment relies heavily on self-care capacity (Feil et al., 2012). In particular, cognitive flexibility and working memory are two executive functions essential for successful management of the disease (Black et al., 2018).

Excitable Axonal Domains

Synaptic inputs into neurons are integrated and converge on an output signal that is transmitted along axons toward the targets. In myelinated axons, action potentials are generated at the axon initial segments (AIS) (Bender and Trussell, 2012; Kole and Stuart, 2012), then regenerated at the nodes of Ranvier (Franssen and Straver, 2013) allowing a rapid and efficient relay of information (Figure I). Together the AIS and the nodes of Ranvier are called the excitable axonal domains.

Axon initial segment

Excitable axonal domains share nearly identical molecular organization—including ion channels, cytoskeletal and scaffolding proteins (Figure II). The axon initial segment (AIS) is a 20-60 μm long neuronal domain traditionally viewed to be situated between the soma and the axon proper (Huang and Rasband, 2018). The formation of the AIS is orchestrated by submembranous scaffolding protein ankyrinG (Figure IIB, (Griggs et al., 2017; Nelson and Jenkins, 2017)). AnkyrinG has multiple binding partners that include the cytoskeletal proteins βIV spectrin and αII spectrin, cell adhesion molecule NF186, and voltage-gated ion channels, including sodium (Nav), potassium (Kv), and calcium (Cav) (Pan et al., 2006; Susuki et al., 2016; Huang et al., 2017; Nelson and Jenkins, 2017). These ion channels regulate membrane properties of the AIS to ensure efficient generation of action potentials.

Emerging evidence indicates that activity-dependent functional plasticity of AIS plays a key role in maintaining neural circuit activity (reviewed in (Yamada and Kuba, 2016; Jamann et al., 2018)). For example, deprivation of auditory input to avian brainstem

auditory neurons caused AIS elongation, which was associated with increased neuronal excitability, presumably as an adaptive response to compensate for the loss of auditory nerve activity (Kuba et al., 2010). Similarly, AIS elongation was observed after sensory deprivation in developing visual cortex (Gutzmann et al., 2014). This homeostatic plasticity is proposed to be a mechanism that maintains network excitability by modulating neuronal output in response to neuronal input changes.

AIS disruption in the central nervous system (CNS)

Recent human studies identified that disruption of the AIS is a key pathophysiological event in various psychiatric and neurological disorders. For example, one of the most significant genetic risk loci for schizophrenia is *ANK3* (Athanasiu et al., 2010; Roussos et al., 2012), a gene that encodes the master organizer for AIS assembly, ankyrinG (Nelson and Jenkins, 2017). Compared to the post-mortem brains of healthy controls, ankyrinG signal intensity is decreased at the AIS of pyramidal neurons in the superficial cortical layer of schizophrenic patients (Cruz et al., 2009). In addition, the number of AIS is dramatically reduced in surviving cortical tissue adjacent to microinfarcts in humans (Coban et al., 2017). Structural alterations such as decreased AIS length or AIS loss are also reported in animal models of various brain diseases, such as stroke (Schafer et al., 2009; Hinman et al., 2013), mild traumatic brain injury (Baalman et al., 2013; Greer et al., 2013; Vascak et al., 2017), Alzheimer's disease (Marin et al., 2016), and multiple sclerosis (Hamada and Kole, 2015; Clark et al., 2016a). Thus, structural changes in the AIS are emerging as a new target of axonal plasticity and/or pathology common in a wide variety of neurological and psychiatric disorders.

Nodes of Ranvier

Nodes of Ranvier are 1 μm short gaps between two adjacent myelin sheaths (Figure I, (Rasband and Peles, 2016)). Similar to AIS, nodal proteins include voltage-gated ion channels, anchored securely to the actin cytoskeleton via the ankyrinG-βIV spectrin complex (Figure IID). Immediately adjacent to either side of the node are the paranodes, which are sites of attachment between the axon and myelin sheath. The primary functions of paranodes are to facilitate saltatory conduction, prevent shunting of current, and stop lateral diffusion of ion channels (Rosenbluth, 2009). Paranodal axoglial junctions are formed by cell adhesion complexes consisting of the glycosylphosphatidylinositol protein contactin (Boyle et al., 2001) and contactin-associated protein (Caspr) (Peles et al., 1997; Bhat et al., 2001; Boyle et al., 2001). The cytoplasmic domain of Caspr interacts with axonal adapter protein 4.1B, which in turn links it to the cytoskeletal βII and αII spectrin complex (Figure IID) [reviewed in Susuki et al. (2016)]. Finally, juxtaparanodes are located adjacent to paranodes and are characterized by a high density of voltage-gated potassium channels (mostly Kv1 subtypes).

Nodes of Ranvier disruption in the central nervous system (CNS)

Nodal disruption has been reported in various CNS diseases (reviewed in (Arancibia-Carcamo and Attwell, 2014)). Like AIS, pathological perturbations at the nodes have been linked to schizophrenia due to the critical role of *ANK3* in this disease (reviewed in (Roussos and Haroutunian, 2014)) and lacunar stroke in human patients (Hinman et al., 2015). In a mouse model of major depressive disorder, nodal alterations in corpus callosum were closely associated with the onset of disease (Miyata et al., 2016). Multiple sclerosis, which is associated with early cognitive impairment (Guimarães and Sá, 2012),

can cause early lesions that involve paranodal disruption (Coman et al., 2006; Howell et al., 2006). Finally, paranodal disruption has been reported in ageing primates (Hinman et al., 2006). Thus, similarly to changes in AIS, nodal structural alterations are being explored as key pathological events in neurological and psychiatric disorders.

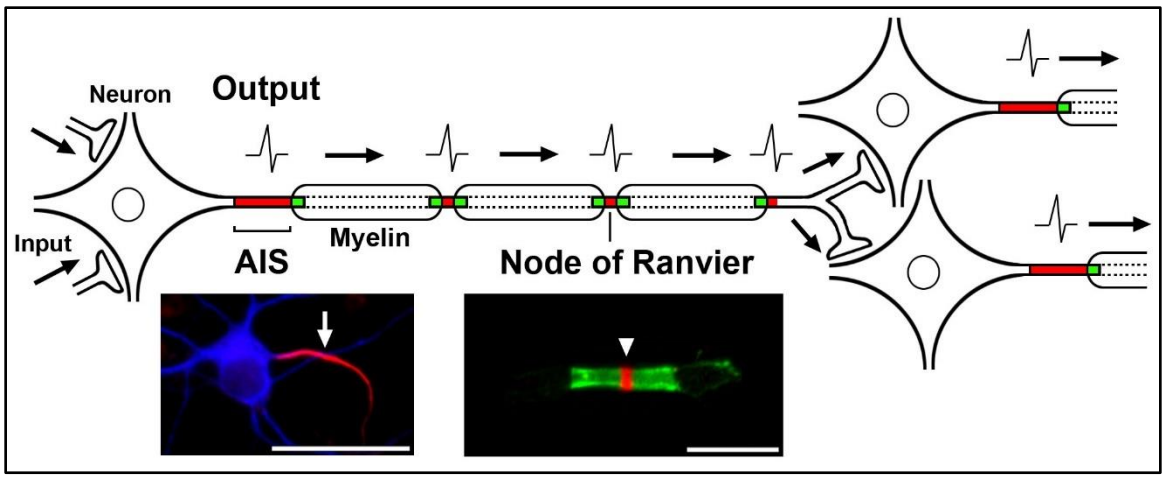

Figure I. Excitable domains along myelinated axons

Figure I. Axon initial segment (AIS) and nodes of Ranvier are the excitable axonal domains required for neuronal output and action potential propagation.

Left panel: Mouse cortical neuron culture stained for AIS (arrow, ankyrinG in red) and somatodendritic domain (MAP2 in blue). Scale bar = 50 μm.

Right panel: Mouse sciatic nerve section stained for node (arrowhead, ankyrinG in red) and paranode (Caspr in green). Scale bar = 10 μm.

This panel is adapted from "Yermakov LM, Hong LA, Drouet DE, Griggs RB, Susuki K (2019) Excitable domains along myelinated axons. Myelin – Basic and Clinical Advances, Springer," in press.

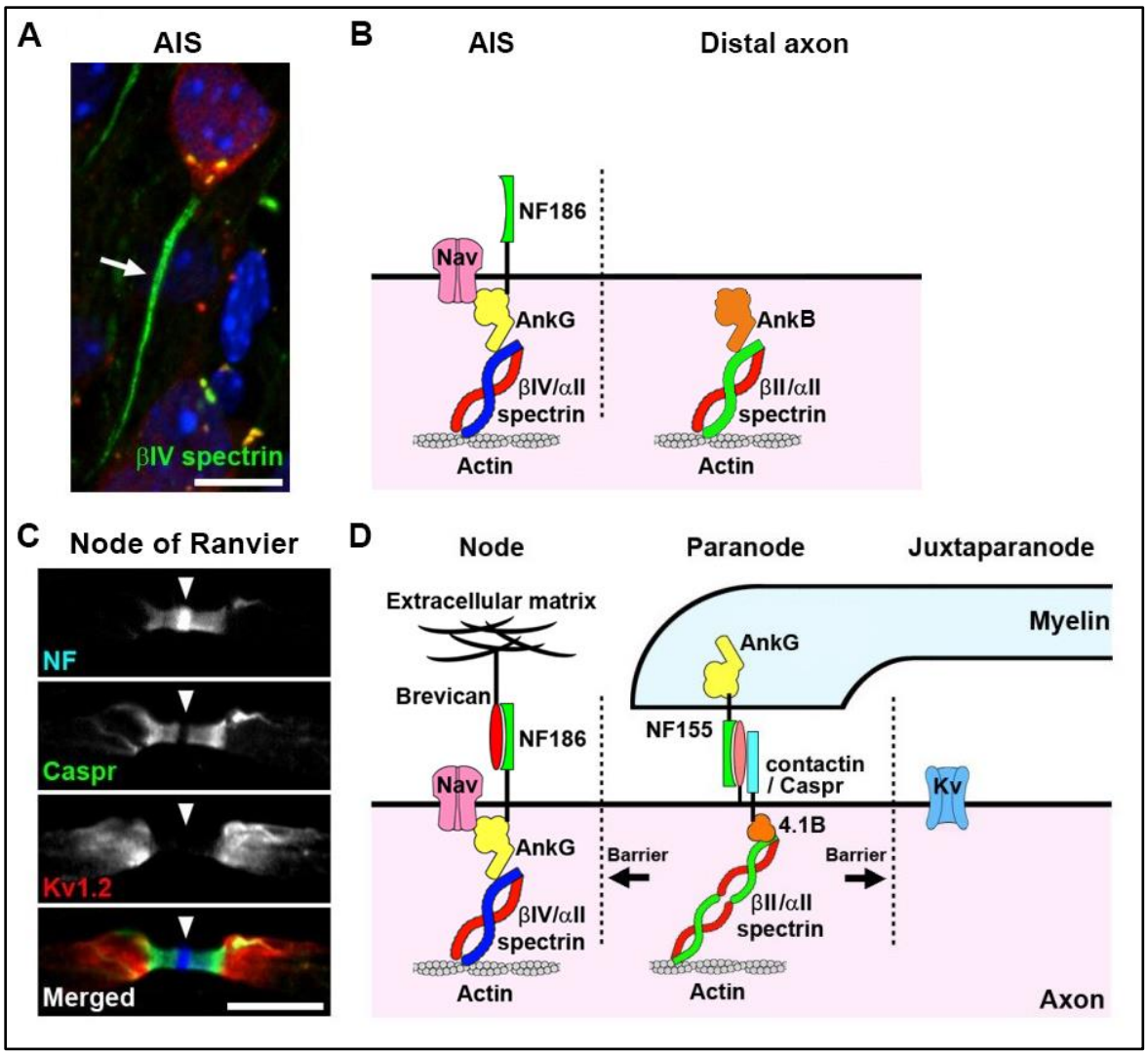

Figure II. Molecular organization of excitable axonal domains

Figure II. **(A)** Representative image of axon initial segment (AIS) in mouse cerebral cortex. AIS (arrow) is labeled in green (βIV spectrin), neuronal soma in red (NeuN), and cell nuclei in blue (Hoechst). Scale bar = 10 μm.

(B) Molecular organization of AIS. The protein complexes at AIS, including voltage-gated sodium (Nav) channels, are secured by the interaction between the axonal cell adhesion molecule NF186. An ankyrinG (AnkG)-βIV spectrin complex links Nav channels to the actin cytoskeleton for further stabilization.

(C) Representative image of node of Ranvier immunostained for neurofascin (NF) in blue, Caspr (paranodal axon) in green, and juxtaparanodal voltage-gated potassium channel (Kv1.2) in red. The antibody to NF stains NF186 at nodal axolemma strongly and NF155 at paranodal glia weakly. Arrowheads indicate node. Scale bar = 10 μm.

(D) Molecular organization of a node of Ranvier. Nodal protein complexes including voltage-gated sodium (Nav) channels are secured by the interaction between the axonal cell adhesion molecule NF186 and extracellular matrix protein brevican. An ankyrinG (AnkG)-βIV spectrin complex links Nav channels to the actin cytoskeleton for further stabilization. Paranodal axoglial junctions are formed by cell adhesion molecules, axonal contactin and contactin-associated protein (Caspr) and glial neurofascin (NF) 155. These junctions act as a diffusion barrier to restrict the mobility of nodal and juxtaparanodal molecules.

This panel is adapted from "Yermakov LM, Hong LA, Drouet DE, Griggs RB, Susuki K (2019) Excitable domains along myelinated axons. Myelin – Basic and Clinical Advances, Springer," in press.

METHODS

Mice

One of the most widely used models for type 2 diabetes is the leptin receptor-deficient *db/db* mice (Chen et al., 1996). Leptin is a hormone produced mostly by adipose tissue, and circulating leptin is taken up into the brain, primarily in the arcuate nucleus of the hypothalamus (reviewed in (Wang et al., 2014a; Fruhwürth et al., 2018)). Leptin acts on the leptin receptor to inhibit hypothalamic neurons that express the appetite-stimulating neuropeptide agouti-related peptide, while simultaneously stimulating nearby neurons that express the appetite-suppressing neuropeptide proopiomelanocortin via JAK/STAT, MAPK, and PI3K signaling pathways. Loss of leptin signaling causes severe hyperphagia leading to obesity and manifest some type 2 diabetes-like characteristics. Indeed, *db/db* mice closely mimic signs in patients with type 2 diabetes such as hyperinsulinemia, obesity and progressive hyperglycemia (Hummel et al., 1966; Coleman and Hummel, 1974).

In this study, male and female *db/db* (BKS.Cg-*Dock7*^{m} +/+ *Lepr*^{db}/J) mice (Jackson Laboratory, Bar Harbor, ME; RRID:IMSR_JAX:000642) aged 5-26 weeks were used. and . Age-matched non-diabetic heterozygote littermates (*db/*+) were used as controls (hereafter referred to as controls). Mice were housed in groups of three to four per cage at 22–24°C with *ad libitum* access to food and water within the Laboratory Animal Resources at Wright State University under 12-h light/12-h dark conditions or in the AAALAC International accredited vivarium at Cincinnati Children's Research Foundation under 14-h light/10-h dark conditions. All animal procedures were approved by the Institutional Animal Care and Use Committee at Wright State University (Animal

Use Protocol # 1113) or at Cincinnati Children's Research Foundation and conform to the United States Public Health Service Policy on Humane Care and Use of Laboratory Animals.

Measurement of blood glucose and Hemoglobin A1c (HbA1c)

A small incision was made on the tip of the tail to obtain a drop of blood. Blood glucose and HbA1c were measured by collecting a drop of blood onto either a TrueMetrix blood glucose test strip (Trividia Health, Fort Lauderdale, FL) or the A1CNow+ blood collection cartridge (PTS Diagnostics, Indianapolis, IN). Blood glucose was measured twice from the same tail incision for better accuracy. For weekly monitored blood glucose levels, the measurements were taken 2-3 hours after the start of the 12-hour light cycle.

Behavioral testing

Behavioral testing was conducted at the Cincinnati Children's Research Foundation Animal Behavioral Core. Behavioral tests with 12-15 mice per group included Morris water maze (MWM) cued training (at 10 weeks of age), MWM spatial working memory version (at 10 weeks), radial water maze (at 11 weeks), MWM acquisition (at 12 weeks), MWM reversal (at 13 weeks), and open-field (at 15 weeks). MWM acquisition was repeated at 24 weeks, followed by MWM reversal at 25 weeks of age. MWM acquisition and reversal were followed by cued-random testing at 13 and 25 weeks of age. Mice could not be tested blindly because of observable differences in body weight; however, only radial water maze was scored manually. Open-field activity was quantified using an automated photobeam system and MWM cued training, spatial working memory,

acquisition, reversal and cued-random outcomes were scored by automated visual tracking software.

Open-field locomotor activity

Mice were tested for locomotor activity in photocell-based automated polycarbonate test chambers (40 cm x 40 cm x 30 cm, PAS system, San Diego Instruments, San Diego, CA). Mouse activity (total number of infrared beam interruptions) and ambulation (successive beam breaks) is reported in 5 min intervals during a 1 h test period.

Morris water maze (MWM)

The test was performed as described (Vorhees and Williams, 2006) with modifications. A white 150 cm diameter polyethylene tank filled halfway with room temperature water (21°C ± 1°C) was used. A white platform was submerged 1.5 cm below the surface of the water, and the size of the platform varied depending on the test phase. Except for cued training and cued-random (during which a proximal cue was placed on the platform), curtains around the pool were opened so that distal cues (geometric shapes and posters on the walls) were visible. Mice were tested in rotation with the inter-trial interval determined by the number of mice being tested at any given time; however, the time was approximately 10 min. Latency and path efficiency (straight-line distance from start to platform ÷ the path taken by the mouse) to reach the goal, along with mean swim speed were measured using Any-Maze video tracking software (Stoelting Instruments, Wood Dale, IL).

MWM cued training

Cued training was given first to acclimate mice to the test requirements and assess swimming ability. Curtains were closed around the pool to obscure distal cues. The escape platform was 10 cm in diameter and contained an orange ball mounted on a steel rod 7 cm above the water to provide a proximal cue to the platform's location. Mice were given six trials with fixed start and platform positions; latency to reach the goal was recorded.

MWM spatial working memory

To assess working memory, two trials per day were administered for 6 days. The location of a submerged 10 cm platform changed every day but did not change between trials, making the task a trial-dependent test of working memory. The first trial on each day was in a new location and represented the sample trial, during which the mouse learned the location of the platform by trial-and-error. The second, test trial, assessed the recollection of the platform location from the sample trial. Improvement of latency or path efficiency between trials 1 and 2 reflects working memory.

MWM acquisition

To assess spatial learning, the submerged platform acquisition phase spanned 5 days with 4 trials per day and a 60 s trial limit. Four quasi-random start positions were used. The submerged platform was 10 cm in diameter and remained in the same location during the 5 days of acquisition.

MWM reversal

To assess cognitive flexibility (i.e., the ability to extinguish the learned platform location used in acquisition and acquire a new location), the submerged platform was moved to

the opposite quadrant from acquisition. A 7 cm diameter platform was used to increase task difficulty; the procedure was the same as acquisition, i.e., 4 trials/day for 5 days, but with different start positions.

MWM cued-random

To assess proximal cue learning, mice were tested in the MWM cued-random procedure. The 10 cm submerged platform was used but it was marked as during cued training with an orange ball mounted on a steel rod that extended 7 cm above the water. Curtains were closed around the pool to obscure distal cues. Whereas during cued training the start and platform were in a fixed location, for cued-random both the start and platform were moved on every trial such that no spatial strategy would be effective. Mice were given 4 trials per day for 2 days and latency to reach the platform was recorded.

Radial water maze (RWM)

To assess working memory, mice were tested using an 8-arm RWM (Hyde et al., 1998). A black 210 cm diameter polyethylene tank was filled halfway with room temperature water (21°C ± 1°C). There was a black 60 cm diameter polyethylene octagon in the center requiring mice to choose an arm by swimming around the octagon. Posters were mounted around the room as distal cues. Each of the maze's 8 arms was 55 cm long and 17 cm wide. At the start of each day, all arms had submerged platforms at the end except for the start arm. Mice were given 7 trials per day for 7 days. After the mouse was placed at the start arm, it was allowed to swim freely for 2 min. After a platform was found, the mouse was given a 30 s rest in a dry cage, and the found platform was removed. If the mouse

failed to find a platform it was given a 2 min rest. An entry into an arm without a platform was counted as a working memory error. An entry into the start arm was counted as a reference memory error. An entry was defined as head and forelegs crossing an imaginary line at the entrance of an arm. The first day of testing in RWM was the training day to teach mice task requirements, therefore day 1 results were not used in the analyses.

Immunohistochemistry

Immunostaining

Mice were sacrificed by isoflurane overdose and brains were immediately removed and fixed in ice-cold 4% paraformaldehyde in 0.1 M phosphate buffer for 90 min, cryoprotected overnight in 20% sucrose, blocked and placed in custom-made foil molds, frozen in TissueTek O.C.T. (4583, Sakura Finetek, Torrance, CA, USA), and stored at -80°C. Coronal brain sections (35 μm) were cut using a cryostat (HM550, Thermo Scientific, Waltham, MA) at 1.7 mm ± 0.15 mm (medial prefrontal cortex), 1.1 mm ± 0.20 mm (corpus callosum) and -1.64 mm ± 0.20 mm (hippocampus) relative to bregma. Staining was performed using free floating sections with gentle rocking. Sections were blocked for 1 h in 0.1 M phosphate buffer (pH 7.4) containing 0.3% Triton X-100 and 10% goat serum (PBTGS), then incubated overnight at 4°C with primary antibodies diluted in PBTGS. Samples were washed 3 times for 10 min in PBTGS, followed by incubation in the dark with fluorescently labeled secondary antibodies for 1 h at room temperature. To detect cell nuclei, sections were counterstained with Hoechst 33342 (Cat# H3570, Thermo Fisher Scientific, IL, USA). Finally, immunolabeled sections were

washed once in PBTGS, and twice in 0.1 M phosphate buffer containing 0.15% Triton X-100, then carefully mounted onto slides using mounting medium (Cat# 71-00-16, KPL, Gaithersburg, MD).

Antibodies

The following primary antibodies were used for immunostaining: mouse monoclonal ankyrinG (N106/36, UC Davis/NIH NeuroMab Facility Cat# 75-146 RRID:AB_10673030), NeuN (Millipore Cat# MAB377 RRID:AB_2298772); rabbit polyclonal Caspr (Abcam Cat# ab34151 RRID:AB_869934), βIV spectrin (M.N. Rasband, Baylor College of Medicine; Texas; USA Cat# βIV SD RRID:AB_2315634), Kv1.2 (Zhang et al., 2013); chicken polyclonal neurofascin (NF) (R&D Systems Cat# AF3235 RRID:AB_10890736). Alexa Fluor (594, 488, 350) or AMCA conjugated secondary antibodies were used (Jackson ImmunoResearch Laboratories, West Grove, PA).

Image capture and AIS measurements

All images were captured on an Axio Observer Z1 with Apotome 2 fitted with a Axiocam Mrm CCD camera (ZEISS, Thornwood, NY). For AIS analysis, three-dimensional z-stack images were taken of the prelimbic area of the medial prefrontal cortex at layers 2-3 (2015 Allen Institute for Brain Science. Allen Brain Atlas. Available from: mouse.brain-map.org. Reference atlas, coronal atlas, image 39 of 132) and pyramidal layer of CA1 of the hippocampus (Allen Brain Atlas, image 72 of 132). In medial prefrontal cortex, AIS measurements were taken from the full mix of glutamatergic and γ-aminobutyric acid (GABAergic) neurons in this region, of which about every 1 out 5 neurons is GABAergic (Hendry et al., 1987; Sahara et al., 2012). In hippocampus, AIS length was measured in

large neurons, most of them are presumably pyramidal cells. Z-stacks were then loaded in Fiji software (Schindelin et al., 2012). Image black and white values of βIV spectrin immunostaining were inverted to display black AIS on white background. AIS were defined as βIV spectrin-labeled segments greater than 10 μm in length with clearly identifiable start and end points. AIS start point was defined as sharply increased βIV spectrin signal closest to the soma. AIS end point was defined as reduced βIV spectrin signal to the point where it could no longer be discerned from the background. AIS that had blunt ends were excluded, as this is likely an artifact of cutting through the AIS during sectioning. The AIS length measurement was performed by carefully tracing the shape of the AIS using segmented line tool in Fiji. The length was measured in around 20 AIS per section, and 3 sections were analyzed per mouse. Measurement of distance from soma to AIS start point was performed as described previously (Harty et al., 2013). In brief, the shortest possible distance between the neuronal soma, identified by NeuN staining, and the most proximal portion of the AIS, identified by βIV spectrin staining, was measured with the straight-line tool in Fiji. Measurement of AIS density was performed per field of view (223.82 × 167.70 μm) in most superficial part of layers 2/3 of the cortex (3 fields of view per animal). For node of Ranvier analysis, nodal gap or paranodal length within the corpus callosum were measured using ZEN 2.3 software (Zeiss). Image quantifications were performed by blinded observers.

Exercise treatment

At 5 weeks of age, *db/db* mice and controls were subjected to forced wheel running using an automated system to control running wheel speed and duration of rotation (Lafayette Instrument, Lafayette, IN) as described previously (Somineni et al., 2014). Mice were trained to run within the wheel over a 5d period. The initial rotation speed of the wheels was set at 4 m/min and increased daily by 1 m/min until a speed of 8 m/min was reached on d5 of training. Similarly, the duration of exercise increased daily from 15 minutes to 1 hour in 15-minute increments. After the last day of training (d5), mice were binned into exercise and no exercise groups. The exercise regimen lasted for 5 weeks from 5 weeks of age until 10-11 weeks of age. Mice in the exercise group were placed in the rotating wheels 7 days/week for 1 h/day at 8 m/min. Exercise sessions took place 2-3 hours before the end of the 12-hour dark cycle. Glucose and weight were monitored weekly. The last glucose and HbA1c measurements were collected at 10 weeks of age, several days before completion of exercise treatment and terminal collection of tissues for immunostaining and western blotting analyses in control and *db/db* mice aged 10-11 weeks. Mice were euthanized at the end of exercise treatment 5 hours after their last exercise session.

Western Blotting

Mice were sacrificed by isoflurane overdose and brains were immediately removed. Frontal lobe and hippocampus were dissected, and flash frozen in liquid nitrogen and stored at -80°C until processing. Brain tissues were homogenized in ice-cold RIPA buffer (25 mM Tris HCl at pH 7.5, 150 mM NaCl, 1% Triton x100, 0.5% Deoxycholate, 0.1% SDS, 10 mM EDTA) using a pestle (BioMasher, Takara Bio USA). Homogenates were

centrifuged at 12,000 rpm (15,000 x g) for 10 min at 4°C in a Sorvall Legend Micro 21R centrifuge (Thermo Scientific). After centrifugation, supernatant was collected into fresh, ice-cold tubes and protein concentrations were measured using a Pierce BCA Protein Assay (Thermo Scientific, Cat# 23225). Samples (10 µg protein) were denatured at 95°C for 5 min in reducing sample buffer (Bio-Rad, Cat# 1610710 and #1610747), then run on a 4–20% Mini-PROTEAN TGX stain-free gel (Bio-Rad, Cat# 4568096). The gel was then transferred to nitrocellulose membrane, 0.45 µm pore size (Bio-Rad, Cat# 1620115). Membranes were blocked with 20 mM Tris, pH 8.0 and 0.05% (v/v) Tween 20 (TBST) containing 4% (w/v) milk for 1 h. Primary antibodies were diluted in TBST with milk at 1:1000, added to the membranes and incubated overnight at 4°C. Primary antibody was washed and horseradish peroxidase (HRP) conjugated secondary antibodies (1:10,000) were incubated for 1 h at room temperature. Signals generated by Pierce ECL Plus Western Blotting Substrate (Thermo Scientific, Cat# 32132) were detected using a ChemiDoc MP Imaging System (Bio-Rad). Quantification of the band density was performed using ImageLab software from Bio-Rad. The densities of the bands of interest were normalized to the relative expression of GAPDH. Total protein staining was used to confirm appropriate protein loading and transfer. Western blotting was performed in collaboration with Domenica Drouet (MS candidate).

Antibodies

The following primary antibodies were used for western blotting: mouse monoclonal NeuN (Millipore Cat# MAB377 RRID:AB_2298772), myelin basic protein (MBP) (BioLegend Cat# 808401, RRID:AB_2564741), GAPDH (Enzo Life Sciences Cat# ADI-CSA-335-E, RRID:AB_2039148); rabbit polyclonal βIV spectrin (M.N. Rasband, Baylor

College of Medicine; Texas; USA Cat# βIV SD RRID:AB_2315634), cleaved caspase 3 (Cell Signaling Technology Cat# 9661, RRID:AB_2341188). Peroxidase conjugated anti-mouse, -rabbit, or -chicken secondary antibodies were used (Jackson ImmunoResearch Laboratories, West Grove, PA).

Statistical Analyses

Behavioral data were analyzed using mixed linear ANOVA models (SAS Proc Mixed, SAS Institute 9.3, Cary, NC). Kenward-Roger adjusted degrees of freedom were used for these models. Diabetes was the between-subject factor and interval or day were the repeated measure factors. Significant diabetes-related interactions were further analyzed using slice-effect ANOVAs. Data are presented as least square (LS) mean ± standard error of the mean (SEM). AIS and nodal data were analyzed using homoscedastic unpaired t-tests (2-tailed) when comparing the means between two groups or using a two-way ANOVA followed by Tukey's multiple comparisons tests for multiple groups. An alpha value of $\alpha=0.05$ was used to determine statistical significance. Correlation between AIS length and levels of blood glucose or HbA1c were analyzed by calculating the Pearson's correlation coefficient. All data were analyzed using Prism 7.0 (GraphPad, La Jolla, CA) and presented as scatter plots with mean ± SEM. Data within Results text is reported as mean ± SEM unless otherwise noted.

SPECIFIC AIM 1 – EXECUTIVE FUNCTIONING IN *DB/DB* MICE

The overall objective of this aim is to establish *db/db* mice as a suitable animal model for testing diabetes-induced impairment of executive functions.

The results described in this chapter are published as "Yermakov LM, Griggs RB, Drouet DE, Sugimoto C, Williams MT, Vorhees CV, Susuki K (2019) Impairment of cognitive flexibility in type 2 diabetic *db/db* mice. Behav Brain Res. doi:10.1016/J.BBR.2019.111978."

Introduction

Intact executive functioning, which includes cognitive flexibility, inhibitory control, working memory, and other abilities (Miyake et al., 2000), is key for successful management of type 2 diabetes. Patients with type 2 diabetes need to keep track of calorie consumption, which requires working memory, and monitor blood glucose levels while performing other tasks, which tasks cognitive flexibility (Black et al., 2018). Therefore, impaired executive functioning in patients with type 2 diabetes (Thabit et al., 2012; Sadanand et al., 2016) could result in poor diabetes management, which could, in turn, exacerbate the impairment of executive functioning (Black et al., 2018) in a vicious positive feedback cycle.

To study type 2 diabetes and its neurocognitive complications, rodent models such as *db/db* mice (Hummel et al., 1966), Zucker Diabetic Fatty (ZDF) rats (Peterson et al., 1990), and rodents given a high-fat diet (Buettner et al., 2006) are commonly used.

Despite the significant impact of impaired executive functioning on patients' life and diabetes management, most studies in diabetic animals focus on the cognitive domain of learning and memory. Spatial learning and memory is commonly assessed using the Morris water maze (MWM) (Li et al., 2002; Gu et al., 2017) and non-spatial memory using novel object recognition (Stranahan et al., 2008; Fu et al., 2017). There are few studies in type 2 diabetic animals assessing cognitive flexibility and working memory, key processes of executive functioning. The few studies that do assess executive functioning raise concerns of confounding effect of severe hypolocomotion of *db/db* mice in land-based tasks, such as the Y-maze (Sharma et al., 2010).

We hypothesized that executive functioning is impaired in type 2 diabetic *db/db* mice. Indeed, here we report significant impairment of cognitive flexibility in 10-week-old *db/db* mice. Impairment in cognitive flexibility tended to worsen with prolonged disease burden at 26 weeks of age in *db/db* mice. We utilize a battery of specialized water-based tasks, such as the radial water maze and the MWM reversal phase to circumvent the hypolocomotion issue observed in land-based tasks. We establish *db/db* mice as a suitable model that parallels impairment in executive functioning observed in patients with type 2 diabetes. This model can be used in the future to develop novel drug therapies and further elucidate the mechanisms of cognitive impairment in type 2 diabetes.

Results

Decreased locomotor activity in db/db mice

Previous studies showed significantly decreased locomotor activity of *db/db* mice starting by 10 weeks of age (Stranahan et al., 2009; Sharma et al., 2010, 2012; Ramos-Rodriguez et al., 2013; Guo and Lu, 2014) In our study, the open-field in 15-week-old mice showed a main effect of diabetes on activity ($F_{(1, 23.5)} = 49.23$, $p < 0.0001$) and a significant diabetes x interval interaction ($F_{(11, 199)} = 3.18$, $p = 0.0005$; Figure 1.1). Similarly, there was a main effect of diabetes on ambulation ($F_{(1, 23.3)} = 47.65$, $p < 0.0001$) and a significant diabetes x interval interaction ($F_{(11, 205)} = 3.19$, $p < 0.0005$; not shown). These data support the idea raised by a previous study (Sharma et al., 2010) that decreased locomotor activity of *db/db* mice could affect the interpretation of land-based tasks such as Y-maze. In contrast, water-based tasks are known to minimize differences secondary to learning, such as locomotor activity or body mass(Vorhees and Williams, 2006). Therefore, to circumvent the problem of hypolocomotion in *db/db* mice, we used water-based tasks to assess executive functions.

MWM cued training

To teach mice to escape and assess swimming ability, MWM cued training was performed first. The *db/db* mice (37.3 ± 2.3 s, n = 15) took longer to locate the platform than the lean controls (26.0 ± 2.6 s, n = 12) ($F_{(1, 48.2)} = 10.77$, $p = 0.0019$). All mice improved over the 6 trials ($F_{(5, 90.1)} = 10.77$, $p = 0.0001$), although there was no interaction with diabetes. The increased latency to locate the platform in *db/db* mice compared with lean controls was likely due to their reduced swim speed (see Figures

1.2B, 1.4B,E). Therefore, to draw conclusions in the following MWM tests, we relied on the swim path efficiency, which is dimensionless (Vorhees and Williams, 2006).

Working memory assessment with MWM and RWM

Using spatial working memory version of the MWM similar to a previously reported method (Cui et al., 2011), we assessed working memory in *db/db* mice known to have diabetes (Hummel et al., 1966). We found a main effect of diabetes on latency during Trial 1 ($F_{(1, 29.8)} = 11.89$, $p = 0.0017$) and Trial 2 ($F_{(1, 30.1)} = 20.70$, $p < 0.0001$; Figure 1.2A) and a main effect of diabetes on swim speed during the same trials (Trial 1: $F_{(1, 23.6)} = 107.02$, $p < 0.0001$; Trial 2: $F_{(1, 25.5)} = 42.11$, $p < 0.0001$; Figure 1.2B). By contrast, path efficiency was not influenced by diabetes on Trials 1 or 2 (Figure 1.2C); no performance improvement was observed between trials. Similarly, RWM did not show a main effect of diabetes (Figure 1.3A) or diabetes x day interaction for working memory errors. There was also no main effect of diabetes on start arm reference errors (Figure 1.3B), but there was a diabetes x day interaction ($F_{(5, 81.8)} = 2.56$, $p = 0.0335$), with *db/db* mice making significantly more start arm reference memory errors on day 7 compared with lean controls (Figure 1.3C). There was no main effect of diabetes (Figure 1.3D) and no diabetes x day interaction for total errors.

MWM spatial learning and flexibility at 12-14 weeks of age

To assess spatial learning in *db/db* mice, MWM acquisition was used (Figures 1.4A-C). We found a significant main effect of diabetes on latency during acquisition ($F_{(1, 25.1)} = 30.64$, $p < 0.0001$), with no diabetes x day interaction (Figure 1.4A). We also found a main effect of diabetes on swim speed ($F_{(1, 25)} = 200.25$, $p < 0.0001$), but no diabetes x day interaction (Figure 1.4B). The *db/db* mice took longer to reach the platform and

swam slower than the control mice. There were no main effects of diabetes or diabetes x day interaction on path efficiency during acquisition (Figure 1.4C). To assess cognitive flexibility, we tested the mice on MWM reversal (Figures 1.4D-F). There was a main effect of diabetes on latency ($F_{(1, 27.6)} = 46.73$, $p < 0.0001$) and a significant diabetes x day interaction ($F_{(4, 77.8)} = 2.68$, $p < 0.0001$; Figure 1.4D), with *db/db* mice taking longer to locate the platform than controls on all days. There was a main effect of diabetes on swim speed ($F_{(1, 25.1)} = 185.91$, $p < 0.0001$) with the *db/db* mice swimming slower than controls, but no diabetes x day interaction (Figure 1.4E). There was a main effect of diabetes ($F_{(1, 26)} = 7.39$, $p = 0.0115$) and diabetes x day interaction ($F_{(4, 82.4)} = 2.98$, $p = 0.0236$; Figure 1.4F) for path efficiency. The *db/db* mice were less efficient than the lean controls on days 4 and 5 of reversal. At the end of reversal in 14-week-old mice, cued-random testing was performed. There was a significant diabetes effect on latency ($F_{(1, 25)} = 12.25$, $p = 0.0018$; not shown) with *db/db* mice taking longer to reach the cued platform than lean controls.

MWM spatial learning and flexibility at 24-26 weeks of age

To determine the effects of prolonged type 2 diabetes on cognitive function, we re-tested the mice in MWM at 24-26 weeks of age. In accordance with a previous study (Ramos-Rodriguez et al., 2013; Pu et al., 2018), acquisition showed a main effect of diabetes ($F_{(1, 25.9)} = 71.25$, $p < 0.0001$) and a significant diabetes x day interaction on latency ($F_{(4, 73.7)} = 2.99$, $p = 0.0241$; Figure 1.5A). *Db/db* mice also showed a significant effect of diabetes on swim speed ($F_{(1, 22.5)} = 123.17$, $p < 0.0001$), but no significant diabetes x day interaction (Figure 1.5B). The *db/db* mice took longer to find the platform and swam slower than control mice. During acquisition, unlike at the younger age (Figure 1.4C),

there was a significant diabetes effect on path efficiency ($F_{(1, 29.2)} = 7.83$, $p = 0.0090$) and a diabetes x day interaction ($F_{(4, 72.5)} = 2.98$, $p = 0.0246$). *Db/db* mice were less efficient at finding the platform than controls during the first two days of acquisition (Figure 1.5C). Next, we assessed reversal in *db/db* mice. We found a significant effect of diabetes ($F_{(1, 22)} = 204.9$, $p < 0.0001$) and diabetes x day interaction on latency ($F_{(4, 67.8)} = 7.58$, $p < 0.0001$; Figure 1.5D). Swim speed showed a main effect of diabetes ($F_{(1, 22.2)} = 212.07$, $p < 0.0001$) with no diabetes x day interaction (Figure 1.5E). The *db/db* mice took longer to locate the platform and swam slower than control mice. Path efficiency showed a significant main effect of diabetes ($F_{(1, 22)} = 20.43$, $p = 0.0002$) and the diabetes x day interaction ($F_{(4, 88)} = 5.83$, $p = 0.0003$). There was a significant reduction in path efficiency during days 2-5 (Figure 1.5F) compared to only days 4-5 in younger *db/db* mice (Figure 1.4F). These results suggest greater impairment of cognitive flexibility in *db/db* mice with advancing age, similar to what is seen in patients (Biessels et al., 2014; Sadanand et al., 2016). At the end of reversal in 26-week-old mice, cued-random testing was performed. There was a significant diabetes effect on latency ($F_{(1, 22.1)} = 76.41$, $p < 0.0001$; not shown) with *db/db* mice taking longer to reach the cued platform than lean controls.

Discussion

For the first time, we report a significant impairment of cognitive flexibility in type 2 diabetic mice. This dysfunction was observed in 13-week-old *db/db* mice, after the development of type 2 diabetes (Hummel et al., 1966). At 24-26 weeks of age, we found sustained impairment of cognitive flexibility. Our findings are relevant to problems with cognitive flexibility found in patients.

There are a number of pitfalls to assessing cognitive function in diabetic rodents. For example, the attention set-shifting task is used to evaluate cognitive flexibility in rodents (Shiers et al., 2018), but food restriction over 3 weeks prior to this test might affect development of diabetes. Previous studies showed decreased locomotor activity in *db/db* mice, and discussed this as a potential confounder of behavioral tasks (Sharma et al., 2010, 2012; Ramos-Rodriguez et al., 2013; Guo and Lu, 2014), whereas another study reported no hypolocomotion in an open-field in *db/db* mice (Wang et al., 2016). Limited locomotor activity in *db/db* mice might be caused by factors other than obesity (Ramos-Rodriguez et al., 2013), although the reason remains unclear. To avoid the pitfalls of food restriction and hypolocomotion observed in *db/db* mice, we utilized water-based tasks, which do not require food restriction and are relatively immune to activity or body mass differences (Vorhees and Williams, 2006). In the MWM, the most commonly reported measure of performance is latency to reach the goal, which could be affected by swim speed. Swim speeds are significantly reduced in *db/db* mice at 10-13 (Figures 1.2B, 1.4B,E), 18 (Zhao et al., 2011), and 24-25 weeks (Figures 1.5B,E) (Infante-Garcia et al., 2017). Although the reason for slower swimming in *db/db* mice is not known, multiple factors such as diabetic polyneuropathy might be involved. Thus, the MWM latency in

db/db mice may not accurately reflect cognitive function. To avoid this problem, we report path efficiency (Figures 1.2C, 1.4C,F and 1.5C,F), a measure that is not sensitive to changes in latency or swim speed (Vorhees and Williams, 2006).

Previous studies and our current results from MWM acquisition show conflicting results of spatial memory deficits in rodent models of type 2 diabetes. ZDF rats did not show spatial learning or memory deficits after 5 or 8 weeks of untreated type 2 diabetes (Bélanger et al., 2004). *Db/db* mice at 7 weeks of age showed a difference only on day-4 of MWM path length with an unadjusted t-test, whereas an overall ANOVA showed no effects on path length (Li et al., 2002). In another study, *db/db* mice at 12 weeks of age had a significantly increased latency compared to control group, although swim speed or path were not assessed (Wang et al., 2016). In the present study, we found no difference in path efficiency of 12-week-old *db/db* mice during MWM acquisition (Figure 1.4C), suggesting that prolonged latency of the *db/db* mice (Figure 1.4A) is mostly due to slow swimming speed (Figure 1.4B). *Db/db* mice at 14 weeks of age showed very limited increase of latency, statistically significant only in the last day of the MWM acquisition phase (Ramos-Rodriguez et al., 2013). Impairment of spatial learning and memory in *db/db* mice might be relatively mild at 7-14 weeks of age, which could lead to the observed variation among the studies. At 26 weeks, latency in MWM acquisition was significantly increased along the entire phase (Ramos-Rodriguez et al., 2013) or in 2nd to 4th days (Pu et al., 2018) in *db/db* mice. In our study, in 24-week-old *db/db* mice, reduced path efficiency in MWM acquisition was observed on days 1 and 2 (Figure 1.5C). This might be due to (i) lack of positive transfer of training in *db/db* mice (i.e. control mice retained the memory of previous task, but *db/db* mice did not), or (ii)

worsening of *db/db* mouse MWM acquisition performance with age. Although our data do not provide conclusive evidence, both possibilities suggest that *db/db* mice show age-dependent memory disturbance as suggested before (Ramos-Rodriguez et al., 2013). We also did not find disturbance in working memory by MWM spatial working memory (Figure 1.2) or RWM (Figure 1.3) in *db/db* mice. In contrast, impairment of cognitive flexibility in *db/db* mice was clearly shown by decreased path efficiency in MWM reversal at 13 (Figure 1.4F) and 25 weeks (Figure 1.5F).

Taken together, our findings in *db/db* mice as well as previous observations in patients with type 2 diabetes suggest that executive functioning, and cognitive flexibility in particular, is one of the impaired cognitive domains in the diabetic brain. *Db/db* mice could provide a useful model to test the effects of new treatment strategies to improve executive functioning during type 2 diabetic condition. To evaluate spatial learning and executive functions in *db/db* mice without the confound of slower swim speeds, future studies should assess path efficiency in MWM acquisition and reversal tasks.

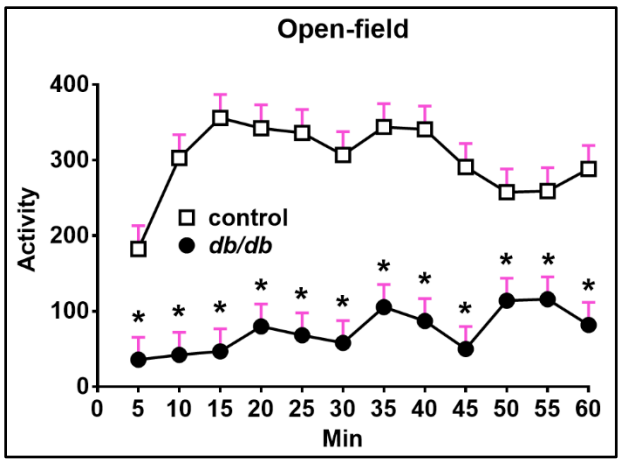

Figure 1.1. Decreased locomotor activity of db/db mice in open-field

Figure 1.1. Data collected in 5 min intervals over a span of 60 min.

All values are LS Mean ± SEM. Group sizes: control = 12; *db/db* = 13. Mice were 15 weeks old at the time of testing. *$p \leq 0.05$ vs. control.

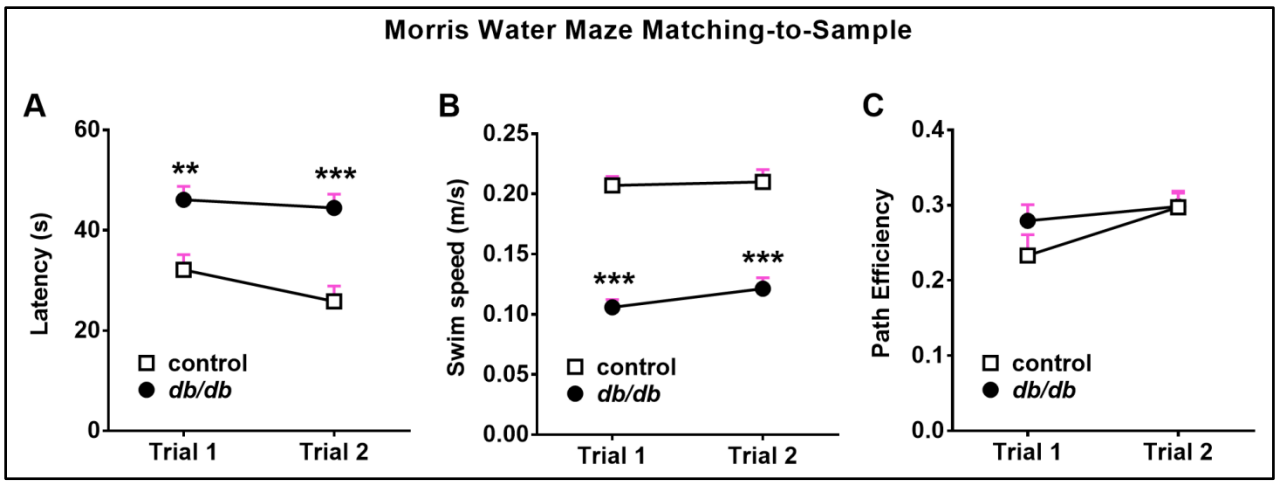

Figure 1.2. Db/db mice performance on Morris Water Maze spatial working memory task

Figure 1.2. **(A)** *Db/db* mice had significantly longer latencies than lean controls in both trials.

(B) *Db/db* mice had significantly slower swim speeds in both trials.

(C) There was no difference in path efficiency. All values are LS Mean ± SEM. Group sizes: control = 12; *db/db* = 15. Mice were 10 weeks old at the time of testing. $^{**}p < 0.01$, $^{***}p \leq 0.001$ when compared with controls.

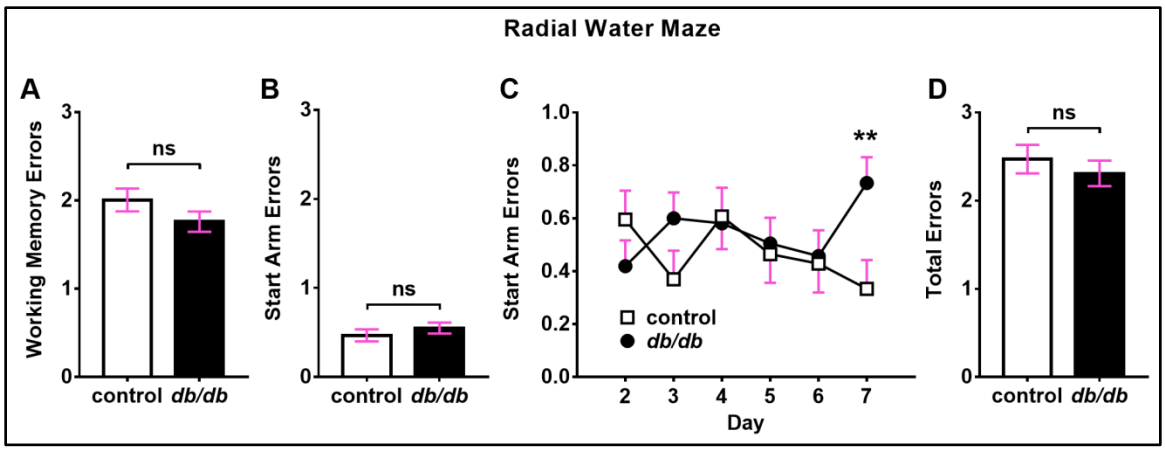

Figure 1.3. Db/db mice performance on Radial Water Maze task

Figure 1.3. **(A)** There was no difference in the number of working memory errors between *db/db* and lean controls.

(B) There was no difference in the number of start arm errors between *db/db* and lean controls.

(C) *Db/db* mice had significantly more start arm errors on day 7, but not on days 2-6.

(D) There was no difference in the number of total errors between *db/db* and lean controls. All values are LS Mean ± SEM. Mice were 11 weeks old at the time of testing. Group sizes: control = 12; *db/db* = 15. $^{**}p \leq 0.01$, vs. control. ns = not significant.

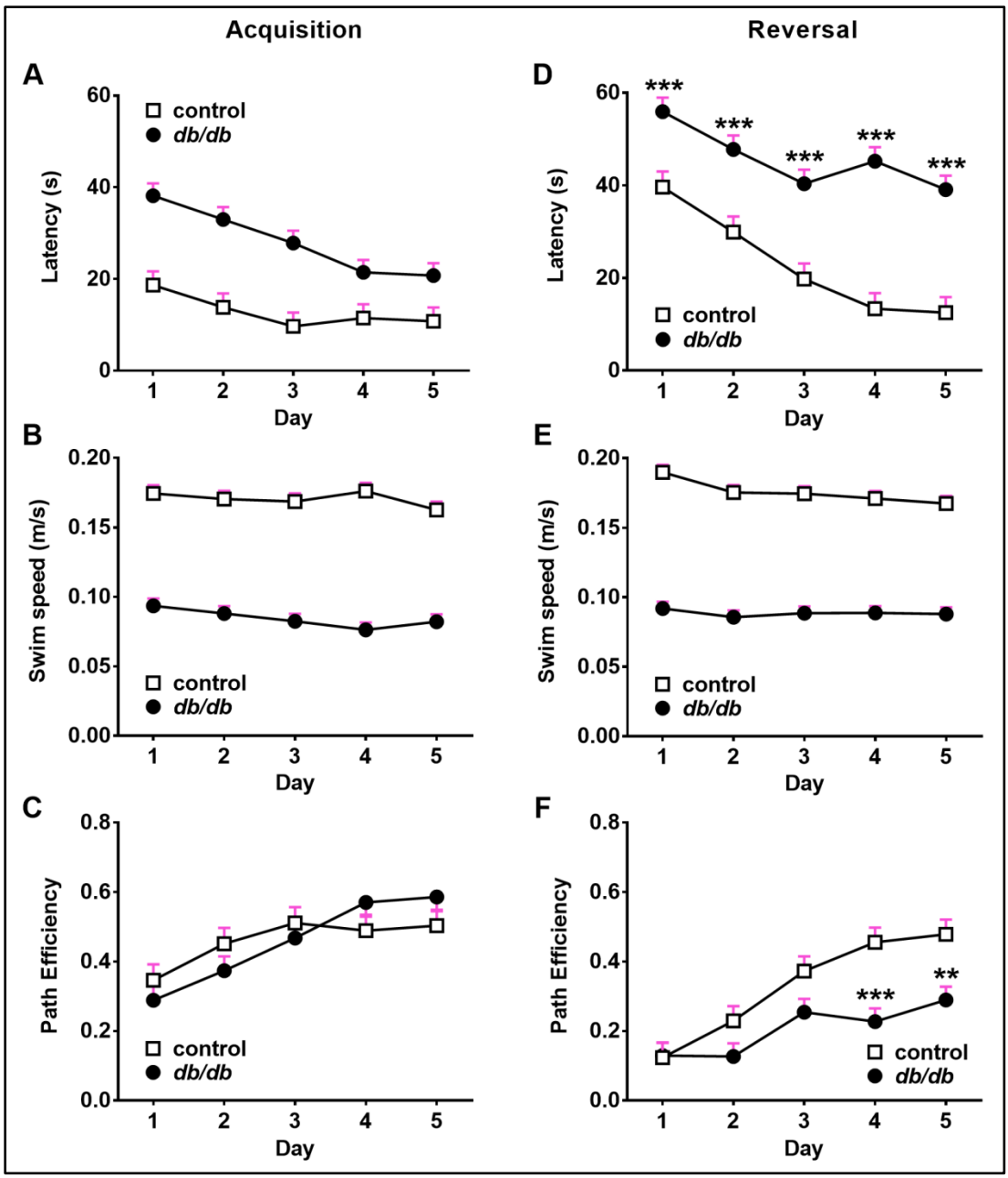

Figure 1.4. 10-week-old db/db mice performance on Morris Water Maze task

Figure 1.4. MWM Acquisition **(A-C)** and Reversal **(D-F)**.

(A) *Db/db* mice had significantly longer latencies to reach the platform than lean controls.

(B) Swim speed stayed constant during acquisition.

(C) Path efficiency was similar in control and *db/db* mice on days 1-5 of acquisition.

(D) *Db/db* mice had significantly longer latencies to reach the platform than lean controls.

(E) Swim speed stayed constant during reversal.

(F) Path efficiency was decreased in *db/db* mice compared to controls on days 4 and 5.

All values are LS Mean ± SEM. Group sizes: control = 12; *db/db* = 15. Mice were 12-13 weeks old at the time of testing. *$p \leq 0.05$, **$p \leq 0.01$, ***$p \leq 0.001$ vs. control.

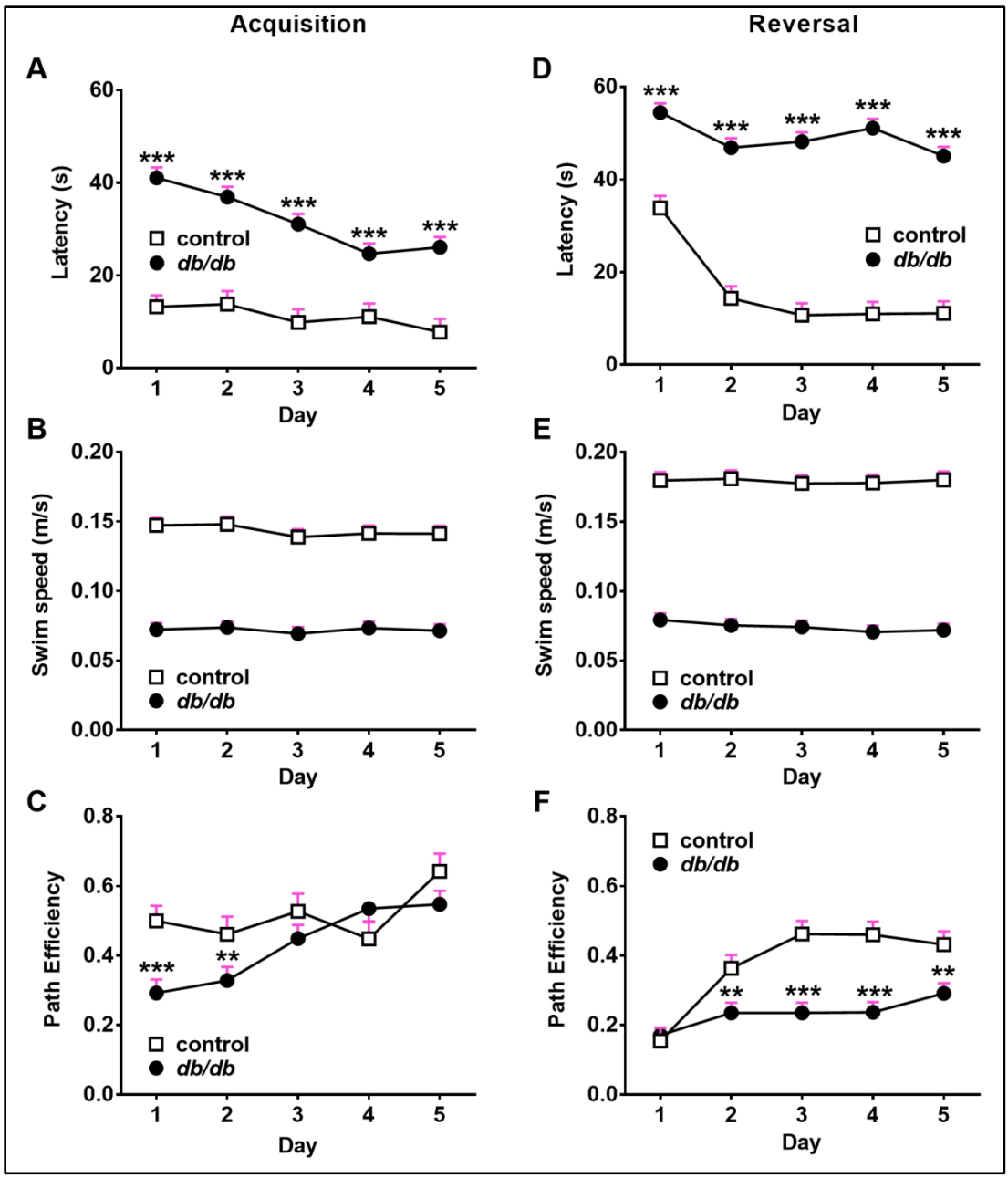

Figure 1.5. 26-week-old db/db mice performance on Morris Water Maze task

Figure 1.5. MWM Acquisition **(A-C)** and Reversal **(D-F)**.

(A) *Db/db* mice had significantly longer latencies to reach the platform than lean controls.

(B) Swim speed stayed constant during acquisition phase.

(C) *Db/db* mice were significantly less efficient than lean controls on days 1 and 2.

(D) *Db/db* mice had significantly longer latencies to reach the platform than lean controls.

(E) Swim speed stayed constant during reversal phase.

(F) Path efficiency was decreased in *db/db* mice compared to lean controls on days 2-5.

All values are LS Mean ± SEM. Group sizes: control = 9 (3 controls excluded due to injuries from fighting); *db/db* = 15. Mice were 24-25 weeks old at the time of testing. $^{**}p \leq 0.01$, $^{***}p \leq 0.001$ vs. control.

SPECIFIC AIM 2 – EXCITABLE AXONAL DOMAINS IN *DB/DB* MICE

The overall objective of this aim is to analyze excitable axonal domains in brain regions associated with cognitive and mood impairment in *db/db* mice.

The results described in this chapter are published as "Yermakov LM, Drouet DE, Griggs RB, Elased KM, Susuki K (2018) Type 2 diabetes leads to axon initial segment shortening in *db/db* mice. Front Cell Neurosci 12:146. doi:10.3389/fncel.2018.00146" and "Yermakov LM, Griggs RB, Drouet DE, Sugimoto C, Williams MT, Vorhees CV, Susuki K (2019) Impairment of cognitive flexibility in type 2 diabetic *db/db* mice. Behav Brain Res. doi:10.1016/J.BBR.2019.111978."

Introduction

Type 2 diabetes is associated with increased risk of developing mild cognitive impairment, mood disorders and dementia, and interferes with the daily life of patients (Stoeckel et al., 2016). Studies in patients with type 2 diabetes indicate functional and neuroanatomical abnormalities in prefrontal gray matter (Kumar et al., 2008) and hippocampus (Gold et al., 2007). Detailed mechanism of how diabetes leads to these and other neurological complications is not fully understood. Previous studies investigating diabetic brain complications focused mainly on neuronal loss (Ramos-Rodriguez et al., 2013; Wang et al., 2016; Infante-Garcia et al., 2017) or altered *neuronal input* in the form of synaptic plasticity (Li et al., 2002; Stranahan et al., 2008) although normal brain

function relies on both neuronal input and output signals. The impact of type 2 diabetes on *neuronal output* remains a critical gap in knowledge.

The key structures for neuronal output are the excitable axonal domains: the axon initial segments (AIS) and the nodes of Ranvier. Synaptic inputs into the neuron are integrated and converge on the initiation of action potentials at the AIS that are propagated along myelinated axons via the nodes of Ranvier (Bender and Trussell, 2012; Kole and Stuart, 2012). Thus, excitable axonal domains contribute to transmitting information and enabling network communication between neurons. Importantly, changes in AIS structures (length and/or location), as detected by ankyrinG or βIV spectrin immunofluorescence, alter excitability and firing behavior of neurons (reviewed in (Yamada and Kuba, 2016; Jamann et al., 2018)). Similarly, structural alterations at the nodes or the flanking paranodes, as detected by neurofascin 186 and Caspr immunofluorescence, can influence conduction velocity along the axons (Babbs and Shi, 2013).

We hypothesized that excitable axonal domains are disrupted in the brain regions associated with cognitive and mood impairment in type 2 diabetic *db/db* mice. Indeed, here we report AIS shortening in both prefrontal cortex and hippocampus in 10-week-old *db/db* mice and additional disruption of nodes of Ranvier along the corpus callosum at 26 weeks of age. These results provide new insights into pathophysiology of neuropsychiatric complications in type 2 diabetes.

Results

AIS length is reduced in db/db mouse prefrontal cortex

To test the hypothesis that type 2 diabetes leads to structural alteration of the AIS, we first analyzed the brains of female *db/db* mice at 10 weeks of age. These *db/db* mice had profoundly elevated blood glucose levels (529.8 ± 32.3 mg/dL, n=3 mice) compared to controls (138.5 ± 2.5 mg/dL, n=3 mice) [p=0.0003, unpaired t-test], as previously reported (Hummel et al., 1966). To visualize AIS structures, we immunostained coronal brain sections with antibodies to the AIS proteins ankyrinG or βIV spectrin. In medial prefrontal cortex of both control and *db/db* mice, overall structures of neurons and AIS were mostly preserved (Figure 2.1A,B). However, the length of the AIS was significantly decreased in *db/db* (24.52 ± 0.48 μm, n=3 mice) compared to control (26.65 ± 0.35 μm, n=3 mice) mice [p=0.0232, unpaired t-test] (Figure 2.1C). The cumulative frequency plot of individual AIS lengths in *db/db* mice showed a leftward shift and a distribution similar to control mice (Figure 2.1D). We also checked for altered location of the start of the AIS relative to the soma, as both proximal and distal shifts of the AIS are recognized as mechanisms of axonal functional plasticity (reviewed in (Yamada and Kuba, 2016; Jamann et al., 2018)). There was no difference in distance from soma to AIS start point between control (1.245 ± 0.0207 μm, n=3 mice) and *db/db* (1.209 ± 0.0158 μm, n=3 mice) mice [p=0.2466, unpaired t-test] (Figure 2.1E). These results demonstrate that AIS shortening, but not AIS relocation, occurs in the medial prefrontal cortex of type 2 diabetic *db/db* mice.

Development of signs of type 2 diabetes in db/db mice is associated with AIS shortening in the prefrontal cortex

To determine if AIS shortening is associated with the development of type 2 diabetes in *db/db* mice and persists over time, we analyzed metabolic signs of type 2 diabetes as well as the AIS in control and *db/db* mice at three timepoints: beginning of diabetes (5 weeks of age), during fully developed diabetes (10 weeks of age) and after a prolonged disease burden (26 weeks of age). We utilized male mice for these experiments to assess potential sex differences as previously reported in *db/db* brain (Vannucci et al., 2001), and because previous reports showed altered neurobehavioral outcomes in male *db/db* mice at an early age (Specific Aim 1, (Li et al., 2002; Sharma et al., 2010; Dinel et al., 2011)).

First, we measured blood glucose to confirm temporal development of type 2 diabetes. At 5 weeks of age, there was no significant difference in blood glucose (Figure 2.2). At 10 weeks of age, *db/db* mice had profoundly elevated blood glucose (498.9 ± 60.8 mg/dL, n=4 mice) compared to controls (132.6 ± 5.8 mg/dL, n=4 mice) [p=0.0010, unpaired t-test) (Figure 2.2). Similar to 10-week-old *db/db* mice, 26-week-old *db/db* mice were also profoundly hyperglycemic (505.8 ± 60.8 mg/dL, n=4 mice) compared to controls (131.3 ± 8.2 mg/dL, n=4 mice) [p<0.0001, unpaired t-test) (Figure 2.2).

We examined AIS structures by immunostaining brain sections as described above. A potential confound of using *db/db* mice is that AIS shortening could be a byproduct of the *db/db* genetic model, and not the development of diabetes, as they are leptin receptor-deficient (Chen et al., 1996) and leptin signaling is involved in the neuronal and glial

development of mouse embryos (Udagawa et al., 2006). However, at 5 weeks of age we observed no difference in AIS length between control (28.58 ± 0.36 μm, n=4 mice) and *db/db* (28.21 ± 0.65 μm, n=4 mice) mice [*p*=0.6280, unpaired t-test] (Figure 2.3A), suggesting that lack of leptin signaling does not impact AIS formation in *db/db* mice before overt signs of diabetes develop. At 10 weeks of age, AIS length was significantly shorter in male *db/db* mice (22.25 ± 1.20 μm, n=4 mice) compared to controls (26.35 ± 0.97 μm, n=4 mice) [*p*=0.0376, unpaired t-test] (Figure 2.3A), consistent with AIS shortening in 10-week-old female *db/db* mice (Figure 2.1C). To test if prolonged diabetic state affects AIS shortening, we evaluated prefrontal cortex of 26-week-old *db/db* mice. Similar to 10-week-old mice, AIS length was shorter in 26-week-old *db/db* mice (23.87 ± 0.70 μm, n = 4) compared with controls (26.87 ± 1.00 μm, n = 4) in prefrontal cortex [*p*=0.0497, unpaired t-test] (Figure 2.3A). The cumulative frequency plot of individual AIS lengths in prefrontal cortex of *db/db* mice showed a leftward shift in 10 and 26-week-old *db/db* mice (Figure 2.3B).

AIS are shortened in the hippocampus of type 2 diabetic db/db mice

In addition to the cerebral cortex, previous studies indicate that the hippocampus is involved in neuropsychiatric complications associated with type 2 diabetes in patients (Gold et al., 2007) and in *db/db* mice (Li et al., 2002). Therefore, we also investigated whether AIS was shortened in the hippocampus of the same animals used for prefrontal cortex analyses. At 5 weeks of age, there was no difference in AIS length between control (31.03 ± 1.145 μm, n=3 mice) and *db/db* (31.22 ± 0.12 μm, n=4 mice) mice [*p*=0.8546, unpaired t-test] (Figure 2.4A). At 10 weeks, the AIS were significantly shorter in *db/db* (27.56 ± 1.47 μm, n=4 mice) compared to control (32.81 ± 0.68 μm, n=4

mice) mice [*p*=0.0184, unpaired t-test] (Figure 2.4A). AIS length was also shorter in hippocampus of 26-week-old *db/db* mice (24.8 ± 0.68 μm, n = 4) compared with controls (27.19 ± 0.57 μm, n = 3) [*p*=0.497, unpaired t-test] (Figure 2.4A), similar to the AIS in medial prefrontal cortex (Figures 2.1, 2.3).

Nodal units in myelinated axons of type 2 diabetic db/db mice are preserved at 10 weeks but not at 26 weeks of age

The nodal unit, consisting of a node of Ranvier, paranodes, and juxtaparanodes, is a critical functional domain in myelinated axons that is needed for proper axonal conduction and network communication. Importantly, the molecular organization at the node of Ranvier is nearly identical to that at the AIS, including sodium channels, NF186, ankyrinG, and βIV spectrin (Figure II, (Griggs et al., 2017; Nelson and Jenkins, 2017). Furthermore, disruption of nodes of Ranvier has been reported in central nervous system (CNS) diseases, such as schizophrenia (reviewed in (Roussos and Haroutunian, 2014)) or lacunar stroke (Hinman et al., 2015), similar to AIS alterations in these same diseases. Therefore, we examined if nodal units are affected in type 2 diabetic *db/db* mouse brain at 10 and 26 weeks of age. We utilized the corpus callosum because it is a large bundle of node of Ranvier-containing white matter fibers that connects the hemispheres of the brain including the medial prefrontal cortex, and a previous study suggested that nodal alterations in corpus callosum are closely associated with onset of major depressive disorder (Miyata et al., 2016). We visualized the nodal unit using established markers of nodes of Ranvier, paranodes, and juxtaparanodes. Immunostaining of nodal ankyrinG and βIV spectrin appeared normal at 10 weeks (Figure 2.5A). We also examined clusters of voltage-gated potassium channels (Kv1.2) at juxtaparanodes, since juxtaparanodal Kv1.2

was reduced in peripheral nerves in *db/db* mice and in nerve biopsies from type 2 diabetic patients (Zenker et al., 2012). The immunostaining of Kv1.2 channel clusters at juxtaparanodes within the corpus callosum appeared similar in 10-week-old control and *db/db* mice (Figure 2.5B). Next, we examined immunostaining of NF186 at nodes and Caspr at paranodes, the region flanking both sides of the nodes in 10 and 26-week-old mice (Figure 2.6A). The nodal gap, or the distance between two opposing Caspr clusters within a single nodal unit, was similar in 10-week-old control and *db/db* mice (Figure 2.6B). However, the nodal gap was elongated in the corpus callosum of 26-week-old *db/db* mice (1.181 ± 0.031 μm, n = 4) compared with controls (1.04 ± 0.023 μm, n = 4) [p=0.0108, unpaired t-test] (Figure 2.6B). The length of a single paranodal Caspr cluster was also similar in 10-week-old mice, but significantly reduced in 26-week-old *db/db* mice (1.376 ± 0.042 μm, n = 4) compared with controls (1.578 ± 0.035 μm, n = 4) [p=0.0099, unpaired t-test] (Figure 2.6C). This type of disruption at the nodes of Ranvier in 26-week-old *db/db* mice suggests that the nodal elongation might be caused by partial loss of the paranodal axo-glial junctions. Therefore, we show that nodal disruption occurs in 26 but not 10-week-old mice, suggesting that prolonged course of type 2 diabetes is likely necessary to disrupt this domain.

Discussion

The current results are the first to show AIS shortening and nodes of Ranvier disruption (elongation) associated with type 2 diabetes. Our data show AIS shortening occurs in both medial prefrontal cortex and hippocampus in *db/db* mice at 10 and 26 weeks of age, during a period when blood glucose levels are elevated. Despite striking similarity of molecular composition and their function, nodes of Ranvier were not affected in 10-week-old *db/db* mice, but disruption occurred later in the disease course, at 26 weeks of age. Our findings may contribute to the understanding of mechanisms behind impaired cognitive function and mood previously reported in *db/db* mice (Specific Aim 1, (Li et al., 2002; Sharma et al., 2010; Dinel et al., 2011)) and patients with type 2 diabetes (Stoeckel et al., 2016).

What is the functional consequence of AIS shortening in diabetic brain? The 8-16% decrease in AIS length reported herein is likely functionally relevant—a computational model showed that just a 4.5% decrease in AIS length reduces neuronal excitability (Baalman et al., 2013). Similarly, shortening of AIS in hippocampal neuron culture by 25% was associated with dampened neuronal excitability (Evans et al., 2015). Thus, AIS shortening due to diabetic conditions in *db/db* brains observed in this study might be a primary disease pathology that likely results in decreased neuronal excitability, further exacerbating the neuronal dysfunction caused by reduced dendritic spine density (Stranahan et al., 2009; Chen et al., 2014a; Dhar et al., 2014). The idea of pathological AIS shortening in diabetes is further supported by previous reports associating AIS shortening with CNS pathology in rodent models of stroke (Hinman et al., 2013), mild traumatic brain injury (Baalman et al., 2013; Vascak et al., 2017), Alzheimer's disease

(Marin et al., 2016), or multiple sclerosis-related experimental autoimmune encephalitis model (Clark et al., 2016b). Thus, our results strongly suggest that the modulation of neuronal output by AIS shortening is involved in the pathophysiology of neuropsychiatric complications during type 2 diabetes. Future studies could determine the contribution, if any, of AIS shortening to cognitive and mood impairment in *db/db* mice.

In addition to AIS shortening, we observed elongation of nodes of Ranvier along the corpus callosum in 26-week-old *db/db* mice, but not in 10-week-old mice (Figure 2.6), suggesting that this disruption arises with prolonged diabetes burden. These nodal and paranodal abnormalities might explain exacerbated deterioration of cognitive function in older patients (Biessels et al., 2014), as well as in older *db/db* mice (Figure 1.5), since nodal elongation can cause nerve conduction slowing (Babbs and Shi, 2013). Nodal disruption might be indicative of white matter abnormalities as seen in patients with type 2 diabetes (Hsu et al., 2012), since node assembly and maintenance depends on myelinating oligodendrocytes (Rasband and Peles, 2016; Griggs et al., 2017). Indeed, an inverse relationship was observed between executive function and white matter integrity in patients with type 2 diabetes (Manschot et al., 2006; Zhang et al., 2014). Furthermore, adult-onset metabolic stress in oligodendrocytes causes progressive white matter pathology, AIS shortening in entorhinal cortex, and memory deficits (Radecki et al., 2018). Thus, our study highlights an important association of structural changes in myelinated axons and cognitive dysfunction related to diabetes.

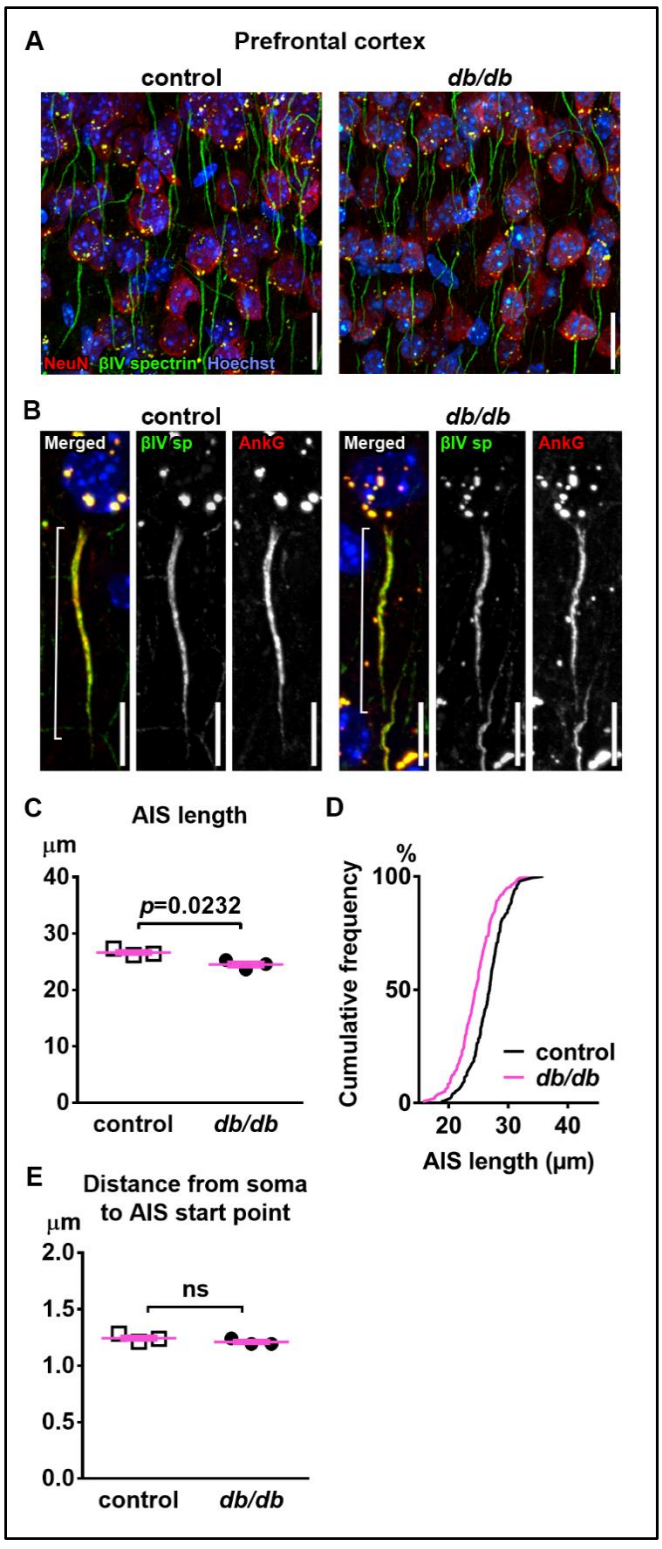

Figure 2.1. Db/db mice have shortened AIS in medial prefrontal cortex

Figure 2.1. **(A)** Representative images depicting the medial prefrontal cortex, prelimbic area, in 10-week-old female control (left) and *db/db* (right) mice. Brain sections were labeled for βIV spectrin (green, AIS), NeuN (red, neuronal soma) and Hoechst (blue, cell nuclei). Scale bars = 20 μm.

(B) High magnification images of a single neuron and its AIS, labeled for βIV spectrin (green, AIS), ankyrinG (red, AIS) and Hoechst (blue, cell nuclei). Brackets show AIS length. Scale bars = 10 μm.

(C) AIS length in medial prefrontal cortex of 10-week-old female *db/db* mice was shorter than controls (n=3 mice in each group).

(D) Cumulative frequency distribution plot of AIS lengths in medial prefrontal cortex shows a leftward shift with no change in shape in *db/db* mice compared to controls. Control, total 194 AISs from 3 mice; *db/db*, total 157 AISs from 3 mice.

(E) Distance from soma to AIS start point in medial prefrontal cortex of 10-week-old female control and *db/db* mice was similar (n=3 mice in each group). ns = not significant.

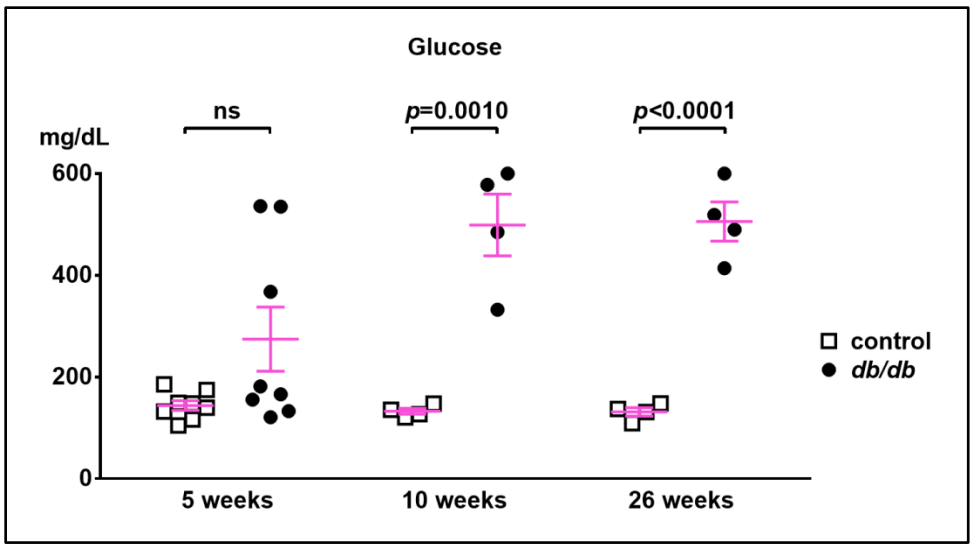

Figure 2.2. Development and persistence of elevated blood glucose in db/db mice

Figure 2.2. Blood glucose levels were similar in 5-week-old male control and *db/db* mice (n=8). They were significantly elevated in both 10 (n=4) and 26-week-old mice (n=4).

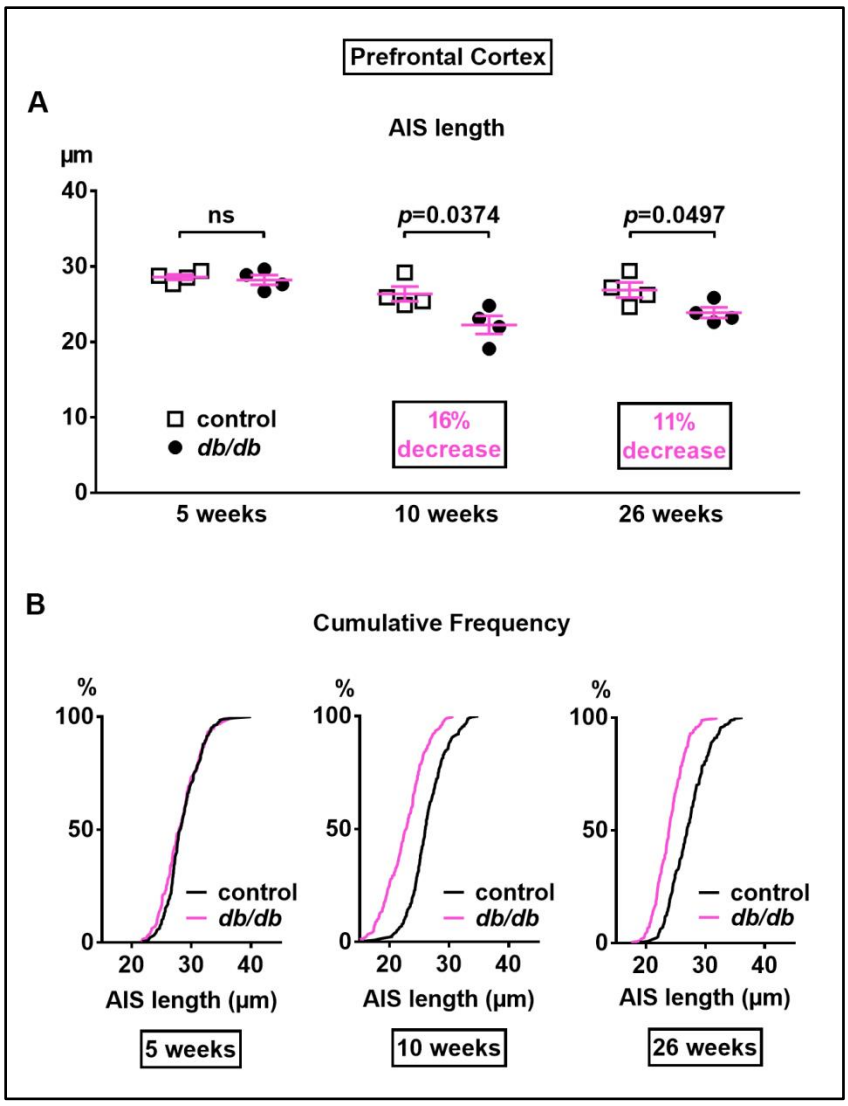

Figure 2.3. Diabetes-related AIS shortening in db/db mouse prefrontal cortex

Figure 2.3. **(A)** AIS length in prefrontal cortex of **5-week-old** control and *db/db* mice was similar (n=4 mice in each group). AIS length in prefrontal cortex of **10-week-old** *db/db* mice was shorter than lean controls (n = 4 mice in each group). AIS length in prefrontal cortex of **26-week-old** *db/db* mice was shorter than lean controls (n = 4 mice in each group).

(B) Cumulative frequency distribution plot of AIS lengths in prefrontal cortex shows similar distribution in control and *db/db* mice at **5 weeks** of age. Control, total 206 AIS from 4 mice; *db/db*, total 193 AISs from 4 mice.

Cumulative frequency distribution plot of AIS lengths in prefrontal cortex shows a leftward shift with no change in shape in *db/db* mice compared to controls at **10 weeks**. Control, total 249 AIS from 3 mice; *db/db*, total 203 AIS from 3 mice.

Cumulative frequency distribution plot of AIS lengths in prefrontal cortex shows a leftward shift in *db/db* mice compared to controls at **26 weeks**. Control total 251 AIS from = 4 mice; *db/db*, total 254 AIS from 4 mice.

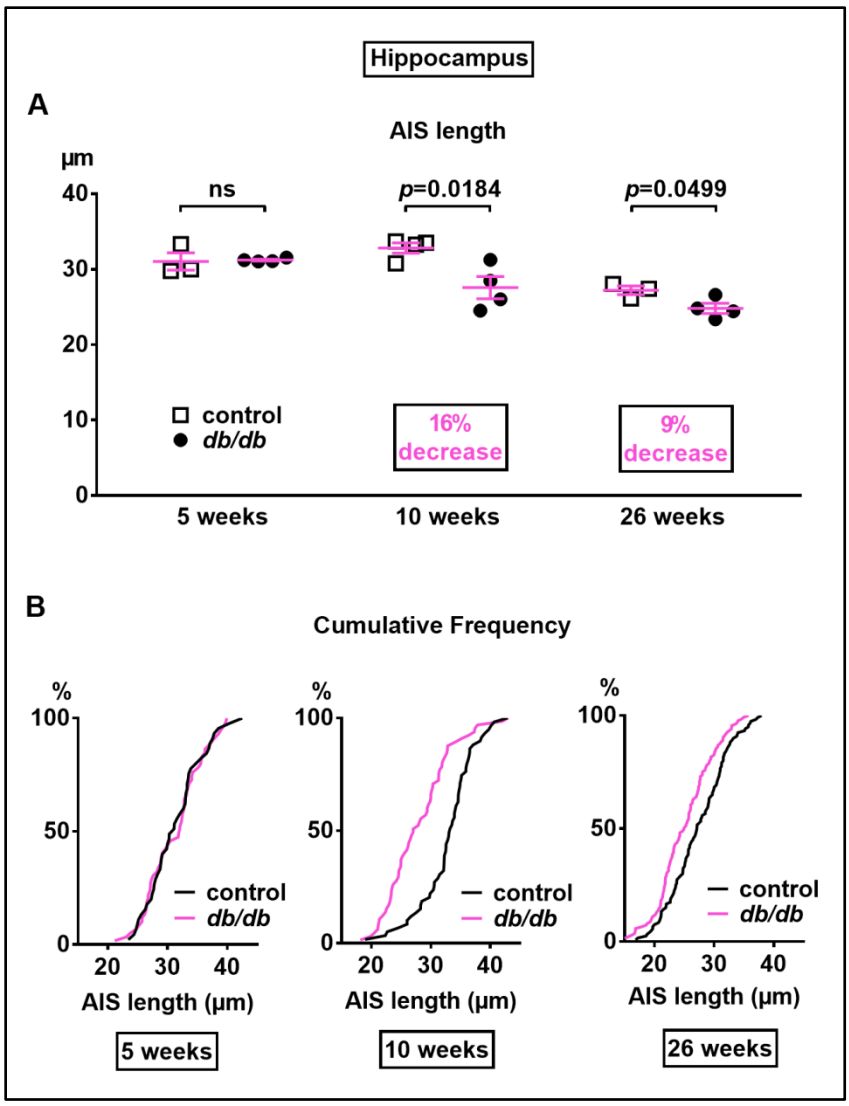

Figure 2.4. Diabetes-related AIS shortening in db/db mouse hippocampus

Figure 2.4. **(A)** AIS length in hippocampus of **5-week-old** male control and *db/db* mice was similar (n=3 mice in control group; n=4 in *db/db* group). AIS length in prefrontal cortex of **10-week-old** *db/db* mice was shorter than lean controls (n = 4 mice in each group). AIS length in prefrontal cortex of **26-week-old** *db/db* mice was shorter than lean controls (n = 4 mice in each group).

(B) Cumulative frequency distribution plot of AIS lengths in hippocampus shows similar distribution in control and *db/db* mice at **5 weeks** of age. Control, total 45 AIS from 3 mice; *db/db*, total 59 AIS from 4 mice.

Cumulative frequency distribution plot of AIS lengths in hippocampus shows a leftward shift in *db/db* mice compared to controls at **10 weeks**. Control, total 59 AIS from 4 mice; *db/db*, total 65 AIS from 4 mice.

Cumulative frequency distribution plot of AIS lengths in hippocampus shows a leftward shift in *db/db* mice compared to controls at **26 weeks**. Control total 120 AIS from 3 mice; *db/db*, total 147 AIS from 4 mice.

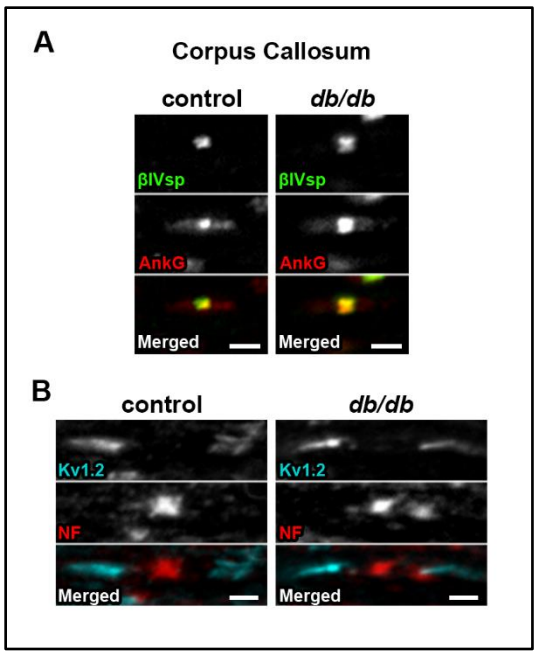

Figure 2.5. Nodes of Ranvier are preserved in corpus callosum of 10-week-old db/db mice

Figure 2.5. **(A)** Representative high magnification images of nodal units in corpus callosum of male control (left) and *db/db* (right) mice at 10 weeks of age. βIV spectrin (βIVsp, green) labels the node and ankyrinG (AnkG, red) labels the node and paranodes. Scale bars = 2 μm.

(B) Representative high magnification images of nodes and juxtaparanodes in corpus callosum of male control (left) and *db/db* (right) mice at 10 weeks of age. Kv1.2 (blue) labeling of the potassium channels at the juxtaparanode appeared similar in control and *db/db* mice. Scale bars = 2 μm.

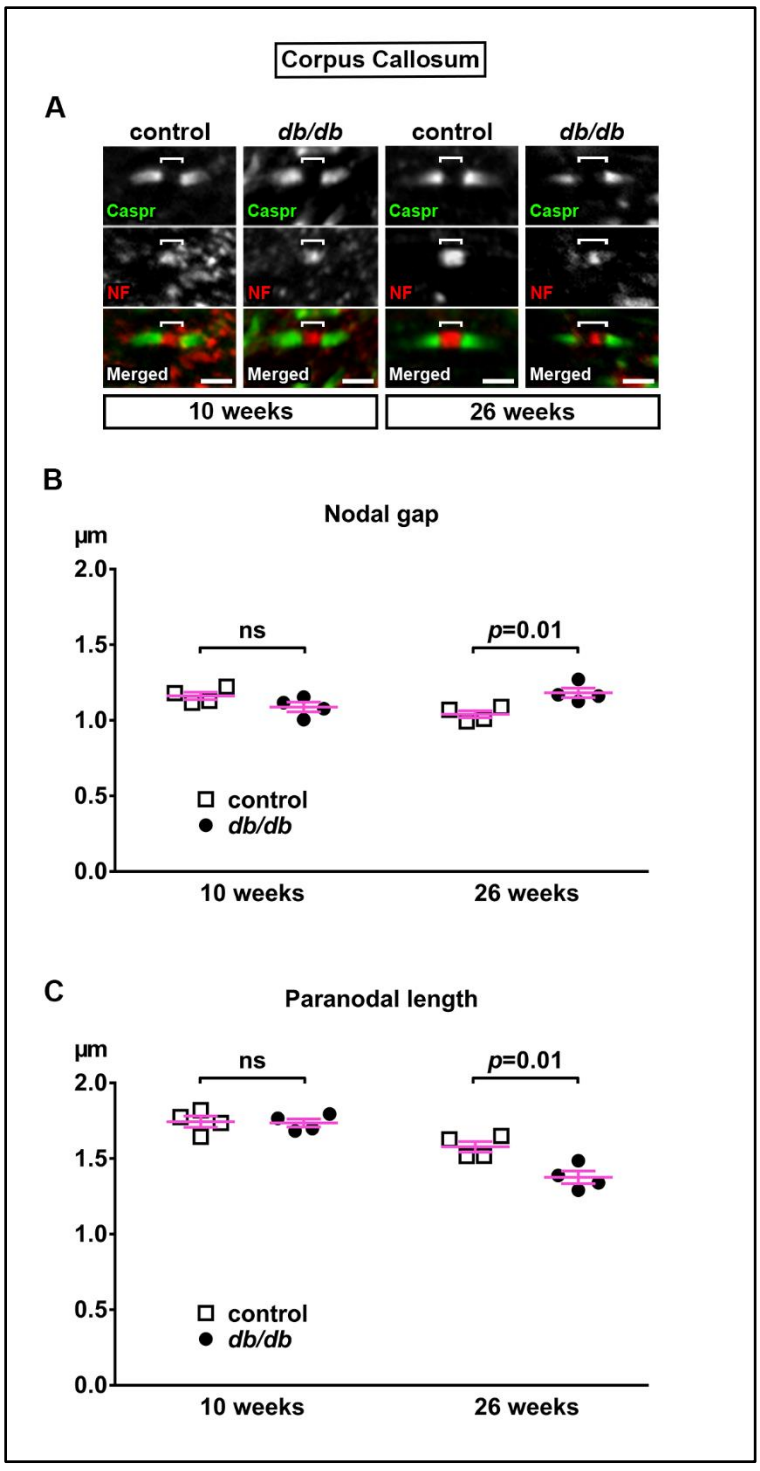

Figure 2.6. Diabetes-related disruption of nodes of Ranvier at 26, but not at 10 weeks

Figure 2.6. **(A)** Representative high magnification images of nodal units in corpus callosum of male control and *db/db* mice at 10 (left) and 26 (right) weeks of age. Caspr (green) labels paranodal junction and neurofascin (NF, red) labels the node. Brackets represent the nodal gap. Scale bars = 2 μm.

(B) The nodal gap, or the distance between two opposing Caspr clusters within a single nodal unit, was similar in control and *db/db* mice at 10 weeks of age (n=4). The nodal gap was elongated in 26-week-old *db/db* mice (500 nodal gaps in each group of n = 4 mice).

(C) The length of a single paranodal Caspr cluster was similar in control and *db/db* mice at 10 weeks of age (n=4). The length of a single paranodal Caspr cluster was shortened in 26-week-old *db/db* mice (1000 paranodes in each group of n = 4 mice).

SPECIFIC AIM 3 –EXERCISE TREATMENT OF *DB/DB* MICE

The overall objective of this aim is to determine if exercise treatment prevents disruption of AIS in *db/db* mice.

The results described in this chapter are published as "Yermakov LM, Drouet DE, Griggs RB, Elased KM, Susuki K (2018) Type 2 diabetes leads to axon initial segment shortening in *db/db* mice. Front Cell Neurosci 12:146. doi:10.3389/fncel.2018.00146."

Introduction

In the previous chapter we have demonstrated that AIS length was significantly decreased in the brains of 10-week-old *db/db* mice compared to age-matched controls, while no difference was observed at 5 weeks of age (Figures 2.3, 2.4). This finding along with development of overt hyperglycemia during the same time (Figure 2.2) suggests that type 2 diabetes causes AIS disruption. However, this is not conclusive. In addition, because of the widespread distribution of leptin receptors in the brain (Leinninger and Myers, 2007), there is a concern that AIS shortening might be a byproduct leptin-receptor mutation in *db/db* mice (Chen et al., 1996).

Exercise has been considered a staple in diabetes management and prevention for decades (Knowler et al., 2002; Sigal et al., 2006). In fact, it has been shown to be more effective than the first-line anti-diabetic medication, metformin, for type 2 diabetes prevention in nondiabetic persons with elevated fasting plasma glucose levels (Knowler et al., 2002). In rodent models of type 2 diabetes, exercise has been shown to improve glucose tolerance

and insulin resistance in mice given a high-fat diet (Boström et al., 2012) or leptin receptor-deficient *db/db* mice (Somineni et al., 2014). Exercise has been utilized as a preventive tool for delaying diabetic nephropathy (Somineni et al., 2014) and preserving dendritic spines in the hippocampus of young *db/db* mice (Stranahan et al., 2009).

We hypothesized that exercise treatment would prevent or slow down the development of type 2 diabetes in *db/db* mice which, in turn, would lead to amelioration of AIS shortening in prefrontal cortex and hippocampus. Indeed, here we report that glucose and HbA1c levels were improved and AIS shortening was not observed in *db/db* mice at the end of exercise treatment. We suggest that development of type 2 diabetes is the cause of AIS shortening in *db/db* mice, which likely plays an important role in disease pathophysiology.

Results

AIS shortening is not observed after exercise treatment

To determine if AIS shortening can be prevented or diminished by treatment of diabetes, we analyzed AIS after anti-diabetic treatment (exercise) from 5 to 10 weeks of age, the period during which elevated blood glucose developed (Figure 2.2).

To attenuate the progression of diabetes, control and *db/db* mice aged 5 weeks were subjected to an exercise regimen using automated running wheel system (Somineni et al., 2014). Exercise treatment in *db/db* mice reduced the temporal development of elevated blood glucose [main effect of exercise in *db/db* mice; $F(1,6) = 8.641$, $p=0.026$]; two-way ANOVA] (Figure 3.1A). There was no difference in HbA1c levels between male control and *db/db* mice at the beginning of exercise, at 5 weeks of age (Figure 3.1B). As expected based on previous studies (Hummel et al., 1966; Sharma et al., 2010), 5-week-old *db/db* mice were at the beginning of diabetes, since HbA1c reflects average blood glucose concentration from approximately the previous 40 days—the average red blood cell lifespan in mice (Wang et al., 2010). Without exercise, HbA1c levels were significantly elevated in 10-week-old *db/db* mice (9.050 ± 0.786 %, n=4 mice) compared to controls (5.850 ± 0.655 %, n=4 mice) [$p=0.0427$, two-way ANOVA followed by Tukey's] (Figure 3.1B). HbA1c levels in exercised *db/db* mice (6.175 ± 0.964 %, n=4 mice) were similar to that in exercised controls (4.625 ± 0.459 %, n=4 mice) [$p=0.4767$, two-way ANOVA followed by Tukey's], confirming the effectiveness of exercise treatment (Figure 3.1B). Neither age or exercise effected blood glucose or HbA1c levels in control mice. After exercise treatment at 10 weeks of age, body weight of the exercised *db/db* mice (42.875 ± 1.102 g, n=4 mice) was similar to that of non-

exercised *db/db* mice (46.15 ± 1.341 g, n=4 mice) [*p*=0.1624, two-way ANOVA followed by Tukey's]. Together, these data demonstrate that exercise treatment attenuated hyperglycemia, providing the appropriate experimental approach to test if the development of type 2 diabetes changes AIS morphology.

Having demonstrated that AIS shortening develops between the ages of 5 to 10 weeks (Figures 2.3, 2.4), we proceeded to test if AIS shortening is ameliorated by exercise treatment starting at 5 weeks. Although the difference in AIS length in the medial prefrontal cortex did not reach statistical significance at the end of exercise between the exercising and non-exercising *db/db* mice [*p*=0.3124], AIS length in exercised *db/db* mice (24.63 ± 0.73 μm, n=4 mice) was similar to that in exercised controls (25.25 ± 0.71 μm, n=4 mice) [*p*=0.9625, two-way ANOVA followed by Tukey's] (Figure 3.2A,B). We also measured AIS in the hippocampus of control and *db/db* mice after exercise treatment. Similar to the medial prefrontal cortex, no AIS shortening was observed in hippocampus of *db/db* mice after exercise treatment: AIS length was similar in exercised control (33.29 ± 1.15 μm, n=4 mice) and exercised *db/db* (31.01 ± 0.65 μm, n=4 mice) mice [*p*=0.4449, two-way ANOVA followed by Tukey's] (Figure 3.3A,B). These results suggest that AIS shortening occurs during the period of development of type 2 diabetes from 5 to 10 weeks of age, whereas AIS shortening does not occur if hyperglycemia is controlled.

Finally, we performed a correlation analysis between AIS length and glucose or HbA1c levels in *db/db* and control mice. There was an inverse correlation between AIS length in the medial prefrontal cortex and blood glucose (r=-0.5327, *p*=0.0336, n=16) (Figure 3.2C) or HbA1c levels (r=-0.485, *p*=0.0569, n=16) (Figure 3.2D). Similarly, we found

significant inverse correlation between AIS length and the levels of blood glucose (r=-0.6567, p=0.0057, n=16) (Figure 3.3C) as well as HbA1c (r=-0.5155, p=0.0410, n=16) (Figure 3.3D) in the hippocampus. These results further support our hypothesis that development of type 2 diabetes leads to AIS shortening in both medial prefrontal cortex and hippocampus, the brain regions that are implicated in development of cognitive impairment and psychiatric symptoms in type 2 diabetic patients.

Neuronal, myelin, or AIS protein levels are unchanged in db/db mice

Progressive cortical atrophy has been reported in *db/db* mice starting at 14 weeks of age (Infante-Garcia et al., 2017). To determine if reductions in neurons, myelin, or AIS protein levels could explain AIS shortening in 10-week-old *db/db* mice, we examined neuronal, myelin, and AIS markers in 10-week-old male control and *db/db* mice (both without exercise) using immunostaining of the prefrontal cortex and western blotting of frontal brain homogenates. The morphology in the prefrontal cortex appeared similar in control and *db/db* mice (Figure 3.4A). The AIS density was similar between control (32 ± 1 AIS / field of view, n=4 mice) and *db/db* (33 ± 2 AIS / field of view, n=4 mice) mice [p=0.6471, unpaired t-test]. Representative immunoblots are shown for NeuN, MBP, βIV spectrin and the loading control protein GAPDH (Figure 3.4B). Consistent with preserved cortical morphology (Figure 3.4A) and AIS density, there was no difference in NeuN or MBP protein level (Figure 3.4C). The immunoblots showed lack of cleaved caspase 3, a marker for apoptotic cell death, in both control and *db/db* brains (Figure 3.4D). Therefore, it is unlikely that the AIS shortening observed in 10-week-old *db/db* mice is due to loss of neurons or myelinated axons. We also found no difference in the protein level of βIV spectrin in the prefrontal cortex (Figure 3.4C). Similar to the medial

prefrontal cortex (Figure 3.4A), NeuN-positive neurons and AIS immunostaining appeared similar in the hippocampus CA1 area in male control and *db/db* mice without exercise (Figure 3.5A). We also examined expression of neuron, myelin, and AIS proteins in hippocampus in 10-week-old male control and *db/db* mice (both without exercise). Consistent with preserved hippocampal morphology (Figure 3.5A), and similar to the prefrontal cortex (Figure 3.4B,C), there were no differences in the protein levels of NeuN, MBP, or βIV spectrin (Figure 3.5B,C), as well as cleaved caspase 3 (Figure 3.5D). Together these findings suggest that in the AIS shortening we observed in prefrontal cortex and hippocampi in 10-week-old diabetic animals is not secondary to gross changes in neurons, myelination, or the AIS protein expression.

Discussion

We report that AIS shortening was not observed after exercise treatment that improved glycemic indices. In addition, AIS length was inversely correlated with signs of type 2 diabetes, such as hyperglycemia and elevated HbA1c. Together with our finding of shortened AIS in 10 but not 5-week-old *db/db* mice, these observations convincingly show that AIS shortening is caused by type 2 diabetes development.

Our results also demonstrated that while hyperglycemia in *db/db* mice was successfully controlled via the exercise treatment (Figure 3.1), the weight of the diabetic animals was not. This is consistent with previous studies that showed beneficial effects of exercise on diabetes and its complications without body weight changes, including improved glycemic control and albuminuria (Somineni et al., 2014), reduced allodynia (Cooper et al., 2017), increased hippocampal dendritic spine density (Stranahan et al., 2009), and prevention of type 2 diabetes in patients with impaired glucose tolerance (Pan et al., 1997). This highlights the importance of exercise as a preventive anti-diabetic treatment, despite its lack of effect on the animal's weight.

We also show that AIS shortening occurred in the absence of changes in the morphological appearance of neurons or in expression levels of neuronal and myelin proteins. Therefore, it is unlikely that AIS shortening observed in 10-week-old *db/db* mice is induced by neuronal loss (Ramos-Rodriguez et al., 2013) or disorganized myelin (Nam et al., 2017) observed in rodent models at more advanced stages of type 2 diabetes. Our results showing no difference in the expression levels of βIV spectrin, despite AIS shortening, are consistent with a previous study in a mild traumatic brain injury model

showing AIS shortening without changes in the levels of AIS proteins (Baalman et al., 2013).

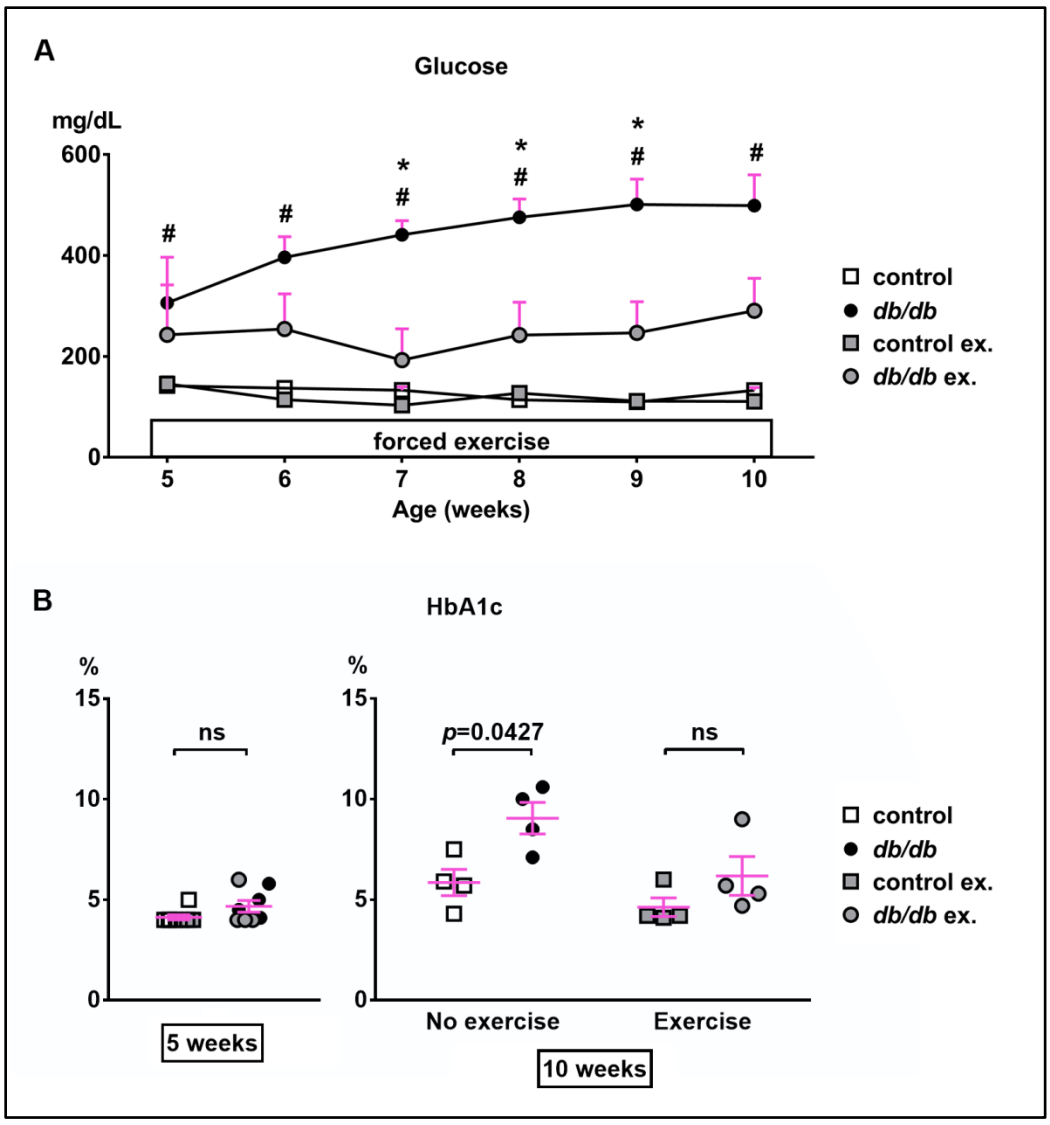

Figure 3.1. Effect of exercise treatment on blood glucose and HbA1c levels

Figure 3.1. **(A)** Blood glucose levels during daily exercise treatment. Exercise attenuated the development of hyperglycemia in *db/db* mice (n=4 mice in each group). # $p<0.05$ for control vs. *db/db*. ***** $p<0.05$ for *db/db* vs. *db/db* exercise.

(B) **Left graph**: HbA1c levels were similar before exercise in 5-week-old control and *db/db* mice (n=8). Gray squares and circles represent mice binned to the exercise group. **Right graph**: HbA1c levels at the end of exercise treatment in 10-week-old mice control and *db/db* mice. Two-way ANOVA [diabetes x exercise: $F(1,12) = 1.245$; $p=0.286$] followed by Tukey's multiple comparisons test yielded the following *p* values: control vs *db/db* [$p=0.0427$], control vs exercise control [$p=0.6548$], control vs exercise *db/db* [$p=0.9891$], *db/db* vs exercise control [$p=0.0055$], *db/db* vs exercise *db/db* [$p=0.0728$], exercise control vs exercise *db/db* [$p=0.4767$].

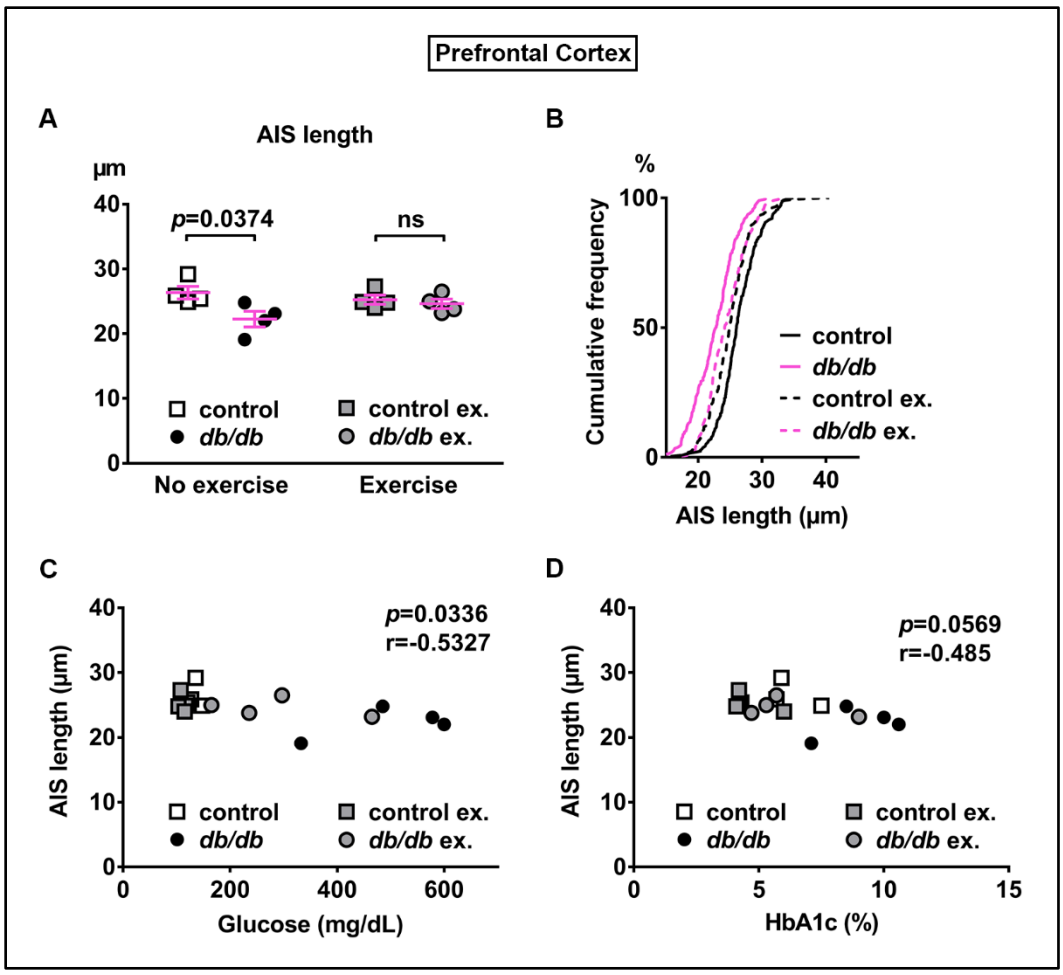

Figure 3.2. Effect of exercise treatment on AIS length in db/db mouse prefrontal cortex

Figure 3.2. **(A)** AIS length in medial prefrontal cortex of control and *db/db* mice with and without exercise treatment (n=4 mice in each group). Two-way ANOVA [diabetes x exercise: $F(1,12) = 3.535$; $p=0.0846$] followed by Tukey's multiple comparisons test yielded the following *p* values: control vs *db/db* [$p=0.0374$], control vs exercise control [$p=0.8338$], control vs exercise *db/db* [$p=0.5686$], *db/db* vs exercise control [$p=0.1537$], *db/db* vs exercise *db/db* [$p=0.3124$], exercise control vs exercise *db/db* [$p=0.9625$].

(B) Cumulative frequency distribution plots of AIS lengths in medial prefrontal cortex of control and *db/db* mice. Control without exercise, total 255 AISs from 4 mice; *db/db* mice without exercise, total 205 AISs from 4 mice; control with exercise, total 213 AISs from 4 mice; *db/db* mice with exercise, total 239 AISs from 4 mice.

(C,D) Scatter plots of mean AIS lengths (y-axis) in relation to levels of blood glucose **(C)** or HbA1c **(D)** (x-axis) of individual mouse at 10 weeks of age.

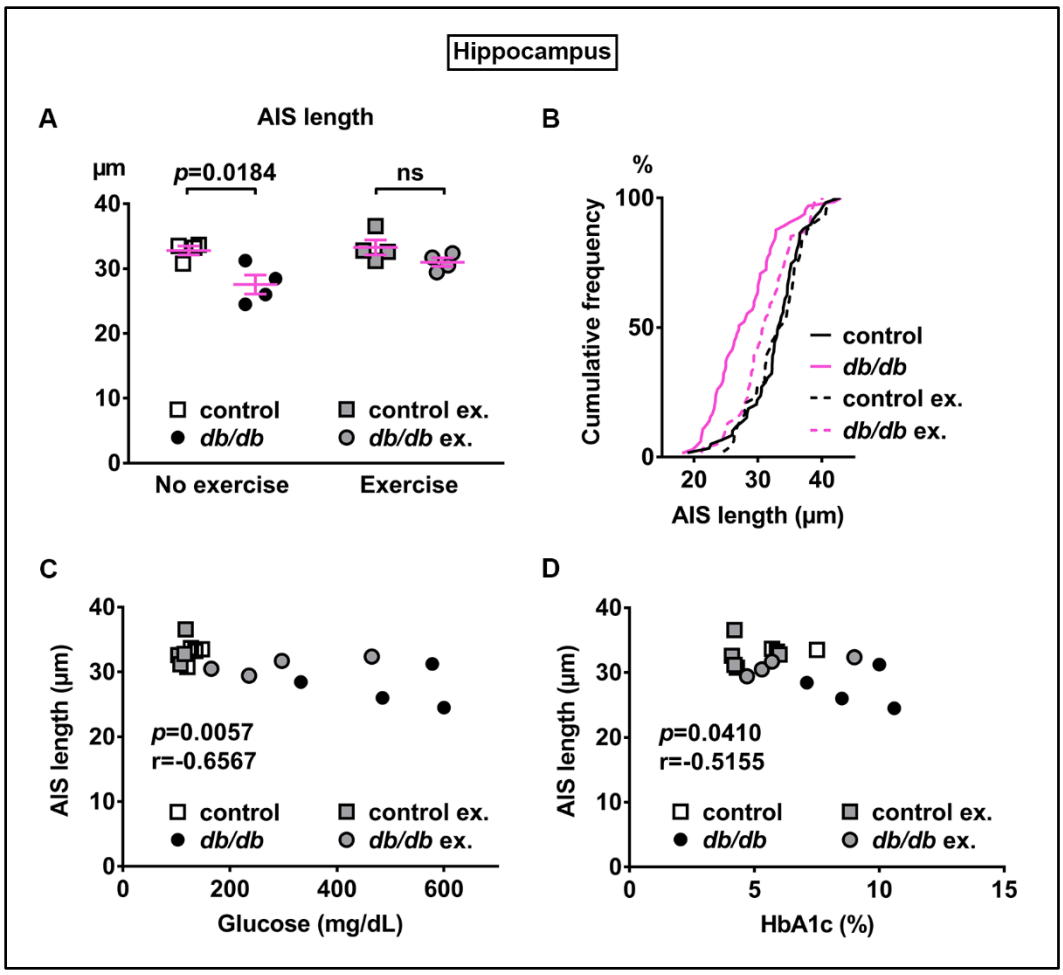

Figure 3.3. Effect of exercise treatment on AIS length in db/db mouse hippocampus

Figure 3.3. **(A)** AIS length in hippocampus of control and *db/db* mice with and without exercise treatment (n=4 mice in each group). Two-way ANOVA [diabetes x exercise: $F(1,12) = 2.002$; $p=0.1825$] followed by Tukey's multiple comparisons test yielded the following *p* values: control vs *db/db* [$p=0.0184$], control vs exercise control [$p=0.9871$], control vs exercise *db/db* [$p=0.6311$], *db/db* vs exercise control [$p=0.0103$], *db/db* vs exercise *db/db* [$p=0.1454$], exercise control vs exercise *db/db* [$p=0.4449$].

(B) Cumulative frequency distribution plots of AIS lengths in hippocampus of control and *db/db* mice. Control without exercise, total 59 AISs from 4 mice; *db/db* mice without exercise, total 65 AISs from 4 mice; control with exercise, total 48 AISs from 4 mice; *db/db* mice with exercise, total 61 AISs from 4 mice.

(C,D) Scatter plots of mean AIS length (y-axis) in relation to levels of blood glucose **(C)** or HbA1c **(D)** (x-axis) of individual mouse at 10 weeks of age.

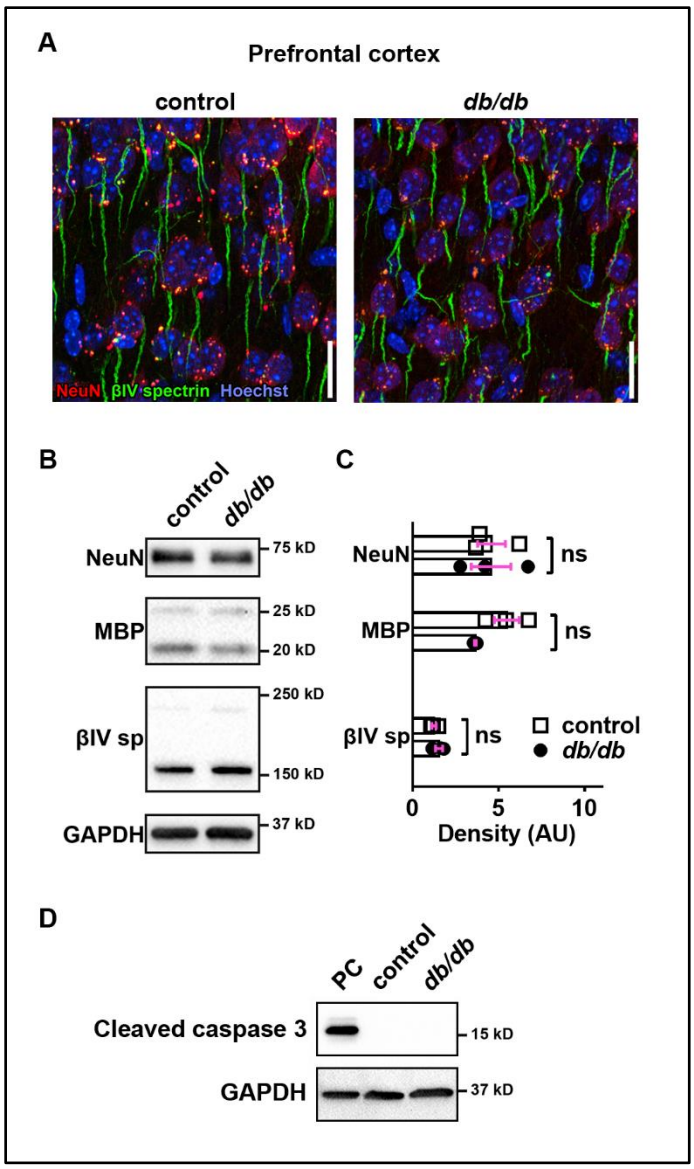

Figure 3.4. No major changes of protein levels in neurons, myelin, and AIS in 10-week-old db/db mouse prefrontal cortex

Figure 3.4. **(A)** Representative images depicting the medial prefrontal cortex, prelimbic area, in 10-week-old male control (left) and *db/db* (right) mice. Brain sections were labeled for βIV spectrin (green, AIS), NeuN (red, neuronal soma) and Hoechst (blue, cell nuclei). Scale bars = 20 μm.

(B) Representative immunoblots of homogenized frontal brain from control and *db/db* mice at 10 weeks of age. βIVsp = βIV spectrin. Uncropped images of the entire original immunoblots are shown in Appendix.

(C) Quantification of relative protein band densities, normalized to GAPDH, and reported in arbitrary units (AU). No difference in protein levels was evident between control and *db/db* mice (n=3). Student's t-tests yielded the following *p* values: NeuN [p=0.9824], both MBP upper and lower bands [p=0.0652], βIV spectrin lower band, βIVΣ6 spectrin, a major isoform in adult brain (Yoshimura et al., 2016) [p=0.2884].

(D) Representative immunoblots of homogenized frontal lobes from control and *db/db* mice at 10 weeks of age. PC = Positive Control, which consisted of Jurkat cells + Cytochrome c (Cell Signaling Technology Cat#9663) and served as positive control for antibody. Uncropped images of the entire original immunoblots are shown in Appendix.

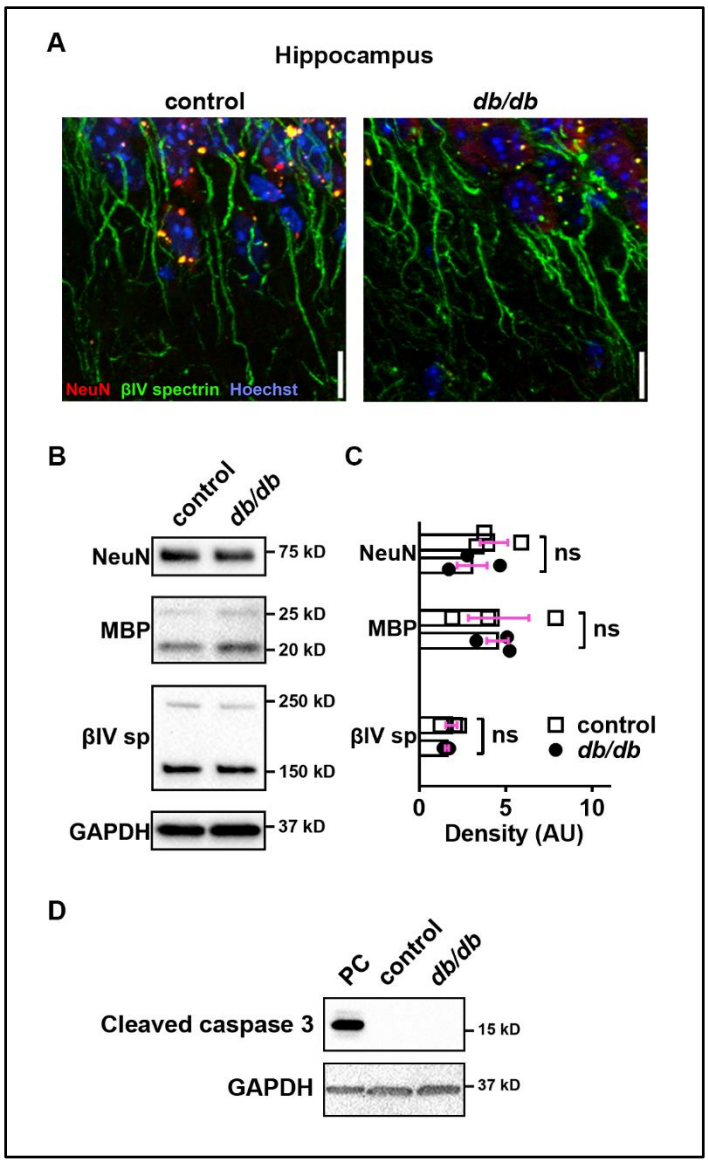

Figure 3.5. No major changes of protein levels in neurons, myelin, and AIS in 10-week-old db/db mouse hippocampus

Figure 3.5. **(A)** Representative images depicting hippocampus, CA1 area, in 10-week-old male control (left) and *db/db* (right) mice (both without exercise treatment). Brain sections were labeled for βIV spectrin (green, AIS), NeuN (red, neuronal soma) and Hoechst (blue, cell nuclei). Scale bars = 10 μm.

(B) Representative immunoblots of homogenized hippocampus from control and *db/db* mice at 10 weeks of age (both with no exercise). βIVsp = βIV spectrin. Uncropped images of the entire original immunoblots are shown in Appendix.

(C) Quantification of relative protein band densities, normalized to GAPDH, and reported in arbitrary units (AU). No difference in protein levels was evident between control and *db/db* mice (n=3). Student's t-tests yielded the following *p* values: NeuN [*p*=0.3401], both MBP upper and lower bands [*p*=0.9782], βIV spectrin lower band, βIVΣ6 spectrin, a major isoform in adult brain (Yoshimura et al., 2016) [*p*=0.4822].

(D) Representative immunoblots of homogenized hippocampus from control and *db/db* mice at 10 weeks of age. PC = Positive Control, which consisted of Jurkat cells + Cytochrome c (Cell Signaling Technology Cat#9663) and served as positive control for antibody. Uncropped images of the entire original immunoblots are shown in Appendix.

CONCLUSION AND FUTURE DIRECTIONS

For the first time, we report significant impairment of cognitive flexibility in type 2 diabetic *db/db* mice. Along with working memory, cognitive flexibility is the key executive function for diabetes management and quality of life in patients (Feil et al., 2012; Black et al., 2018). In addition to previous reports of impaired learning and memory (Biessels et al., 1996; Li et al., 2002; Stranahan et al., 2008; Chen et al., 2014a; Infante-Garcia et al., 2017; Zheng et al., 2017) and depression-like behavior (Li et al., 2002; Sharma et al., 2010, 2012), our finding of impaired cognitive flexibility (Specific Aim 1) establishes *db/db* mice as a model that closely parallels cognitive and mood deficits in patients with type 2 diabetes.

The pathophysiology underlying cognitive and mood dysfunction in type 2 diabetes is unknown. Studies in patients with type 2 diabetes describe neuroanatomical abnormalities in hippocampus (Gold et al., 2007) and prefrontal cortex (Kumar et al., 2008), implicating these regions. Previous studies suggest that type 2 diabetes alters synaptic plasticity in the hippocampus resulting in cognitive deficits in *db/db* mice (Li et al., 2002; Stranahan et al., 2008). In addition, *db/db* mice have reduced dendritic spine density in dentate gyrus granule neurons in the hippocampus (Stranahan et al., 2009), hippocampal CA1 (Chen et al., 2014a) and CA3 pyramidal neurons (Dhar et al., 2014), and layer II/III pyramidal neurons in prefrontal cortex (Chen et al., 2014a). Our current results (Specific Aim 2) demonstrate shortening of the AIS in hippocampal CA1 and layer II/III neurons in prefrontal cortex, as well as elongation of nodes of Ranvier along the corpus callosum. Similar to the effects of exercise treatment in the current study (Specific Aim 3), voluntary running wheel activity attenuated reduction of dendritic spine

density in hippocampus in *db/db* mice (Stranahan et al., 2009). Thus, these structural changes in AIS and nodes of Ranvier together with synaptic loss likely disturb the neuronal network coordination presumably required for appropriate cognitive function in type 2 diabetic *db/db* mice.

The summary of our major findings along with key diabetes-associated events, such as the onset of insulin resistance and cortical atrophy in *db/db* mice, are presented in Figure 4.1.

There are many questions that remain to be answered. For example, one important question is whether the lack of functional leptin receptor in *db/db* mice may contribute to AIS shortening, nodal elongation and cognitive impairment. Leptin signaling plays an important role in neuronal and glial development of mouse embryos (Udagawa et al., 2006). Our data suggests that the AIS shortening in *db/db* mice was not due to disrupted leptin signaling, since diabetes treatment ameliorated AIS shortening (Specific Aim 3). Moreover, a study using leptin-deficient *ob/ob* mice, an established model of obesity but only mild and transient hyperglycemia (Wang et al., 2014a; Giesbertz et al., 2015), showed preserved cognitive flexibility in MWM reversal, as well as preserved dendritic spine density in the hippocampus at 16-24 week of age (Bracke et al., 2019). This further supports the hypothesis that type 2 diabetes condition and not obesity or disturbed leptin signaling is what leads to neurobehavioral deficits and morphological brain changes in *db/db* mice. Analyses of other models of type 2 diabetes, such as high-fat diet commonly used to induce insulin resistance in rodents (Buettner et al., 2006), may be used to address this issue further.

What is the relationship among alterations in synapses, AIS, nodes, and myelin that culminate in cognitive dysfunction in type 2 diabetes? Our results cannot distinguish between AIS shortening as the result of neuronal homeostatic plasticity or as a type 2 diabetes pathology or both. Presumably, reduced dendritic spines would lead to decreased input and compensatory AIS lengthening and/or relocation. However, both AIS shortening (Specific Aim 2) and reduced dendritic spine density (Stranahan et al., 2009; Chen et al., 2014a; Dhar et al., 2014) are reported in similarly aged *db/db* mice displaying cognitive and mood dysfunction (Specific Aim 1, (Li et al., 2002; Sharma et al., 2010)). This suggests that AIS shortening is a pathological change caused by type 2 diabetes, rather than adaptive or compensatory change to maintain neural circuit activities. However, one also needs to consider a scenario in which both AIS shortening and reduction in dendritic spine density could be compensatory to yet another pathological mechanism causing overall network hyperexcitability, as has been recently reported in the case of GABAergic synapse loss at the AIS (Nelson et al., 2018). Similarly, we do not know if the node of Ranvier elongation along corpus callosum in *db/db* mice at 26 weeks is due to diabetes or secondary to brain damage, such as myelin defects, or both. Future studies need to test if long-term diabetes treatment (5-26 weeks) with exercise or established anti-diabetic drug such as rosiglitazone can ameliorate the nodal disruption.

Detailed information on AIS changes in neuronal subtypes (e.g. excitatory vs. inhibitory) is necessary for a comprehensive understanding of disturbed neural circuits under diabetic conditions. Even though it is likely that AIS shortening occurs to a similar degree in all populations of neurons (Figure 2.1D), this is not conclusive, because detailed information for cell-type-specific AIS shortening is lacking. Previous studies

show that neuronal cell-type is important in either diabetic brain complications or AIS morphology. Loss or changes of specific types of inhibitory neurons have been reported in type 2 diabetic Goto-Kakizaki rats (Larsson et al., 2016). AIS length is substantially heterogeneous in interneurons and pyramidal neurons (Höfflin et al., 2017), and the pattern of activity-dependent AIS changes is different between inhibitory interneurons and excitatory neurons (Chand et al., 2015). Cell-type-specific analyses of AIS changes could be an important next step to better understand pathophysiology of diabetic brain complications.

In addition, what are the molecular and cellular mechanisms of excitable axonal domain disruption in diabetic brain? Some researchers propose that type 2 diabetes and Alzheimer's disease might share metabolic dysfunction upstream of the observed cognitive decline (Chornenkyy et al., 2018). Such dysfunction likely begins early in the disease process and might explain cognitive decrements observed among type 2 diabetes patients of all ages (Biessels et al., 2014). Interestingly, type 2 diabetes is clinically associated with both Alzheimer's disease-type and vascular-type dementias (Chornenkyy et al., 2018), and AIS shortening has been reported in mouse models of both Alzheimer's disease (Marin et al., 2016) and cerebrovascular lesions (Hinman et al., 2013; Coban et al., 2017). Potential metabolic disruptors of axonal domains might include mitochondrial dysfunction (Neth and Craft, 2017) or increased glucose metabolite methylglyoxal (Bierhaus et al., 2012), which have been shown to disrupt nodes of Ranvier (Marella et al., 2013; Griggs et al., 2018) and oxidative stress (Verma et al., 2016), which induces AIS disruption (Clark et al., 2017).

Previous studies also indicate that both homeostatic plasticity and pathological alterations of the AIS involve changes in intracellular calcium (Ca^{2+}) levels and calcium-dependent enzymes. Pathological AIS alterations are mediated by calpain, a calcium-dependent cysteine protease, in models of stroke (Schafer et al., 2009), induced excitotoxicity (del Puerto et al., 2015; Benned-Jensen et al., 2016), and multiple sclerosis (Clark et al., 2016b). In addition, hyperphosphorylated tau (Hatch et al., 2017) or oxidative stress followed by calpain activation (Clark et al., 2017) induce pathological alterations of AIS. Calcium/calmodulin-dependent kinase II (CaMKII) may regulate excitability through its interaction with ankyrinG and βIV spectrin complex that anchor it to the AIS (Hund et al., 2010). Interestingly, a study looking at proteomic profile in *db/db* mice found altered expression of CaMKIIα, CaMKIIβ, CaMKIIδ and calcineurin subunit B type 1 both in hippocampus and frontal cortex (Ernst et al., 2013), and post-translational O-GlcNAcylation of CaMKII is increased in the diabetic brain (Erickson et al., 2013). Calcineurin, a calcium/calmodulin-dependent protein phosphatase, is responsible for both activity-dependent relocation (Evans et al., 2013) and shortening (Evans et al., 2015) of the AIS. Furthermore, AIS assembly, maintenance, and/or plasticity may also be regulated by cannabinoid receptors (Tapia et al., 2017), brain-derived neurotrophic factor and neurotrophin 3 (Guo et al., 2017), protein kinase CK2 (Bréchet et al., 2008; Hien et al., 2014; Xu and Cooper, 2015; Lezmy et al., 2017), Cdk5 (Trunova et al., 2011; Chand et al., 2015), microtubule cross-linking factor 1 (Satake et al., 2017), myosin II activity (Evans et al., 2017; Berger et al., 2018), or Rbfox splicing factors (Jacko et al., 2018). Future studies are required to identify the key mechanism of diabetes-related AIS changes. Induction of diabetes in the mutant mice with disruption of these mediators

would be a powerful approach to uncover the key regulator of structural changes in AIS and nodes of Ranvier during diabetic brain complications.

Finally, while our current results demonstrate that excitable axonal domains are affected in association with the development of type 2 diabetes, are the excitable axonal domains modulated in the setting of type 1 diabetes? Similar to type 2 diabetes discussed above, learning and memory deficits are also reported in patients with early-onset type 1 diabetes (Semenkovich et al., 2016a, 2016b). The streptozotocin model of type 1 diabetes is associated with depression (Castillo-Gómez et al., 2015), learning and memory impairment (Biessels et al., 1996; Stranahan et al., 2008), reduced long term potentiation in the prefrontal cortex (Wu et al., 2017), and reduced dendritic spine density in hippocampus (Wang et al., 2014b; Xiang et al., 2015) and prefrontal cortex (Wu et al., 2017). Analyses of human brain tissues are also required to confirm the roles of disrupted excitable axonal domains in the pathophysiology of type 1 as well as type 2 diabetes.

In conclusion, this is the first study to report impairment of cognitive flexibility in type 2 diabetic *db/db* mice. In addition, we report structural changes at the AIS and nodes of Ranvier associated with the development of type 2 diabetes. We report AIS shortening in medial prefrontal cortex and hippocampus, and nodes of Ranvier disruption along the corpus callosum, the brain regions critical for appropriate cognitive function and affect. In addition to the dendritic plasticity modulating *neuronal inputs*, the disruption of excitable axonal domains regulating *neuronal outputs* might contribute to the development of neuropsychiatric symptoms during type 2 diabetes. Thus, treatments aiming to restore these domains might be a novel strategy to ameliorate cognitive and mood impairments in type 2 diabetes.

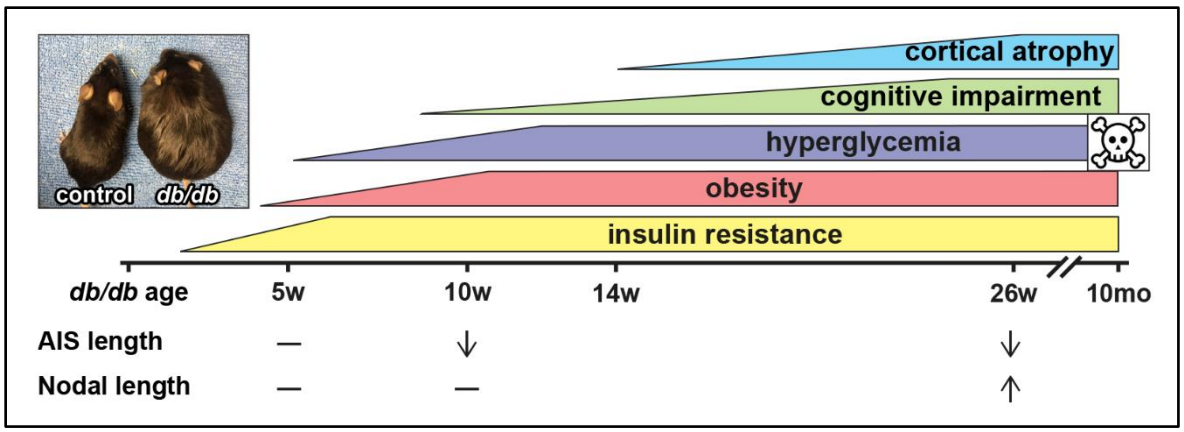

Figure 4.1. Timeline of major diabetes-associated events in db/db mice

Figure 4.1. Db/db (BKS.Cg-*Dock7*^{m} +/+ *Lepr*^{db}/J) mice (Hummel et al., 1966) start to develop insulin resistance around 10-14 days. Obesity starts at 3-4 weeks of age. Hyperglycemia onset is between 4 to 8 weeks. We (Specific Aim 1) and others (Li et al., 2002; Sharma et al., 2010) report cognitive impairment at around 7-10 weeks of age. Progressive cortical atrophy has been reported starting at 14 weeks of age (Infante-Garcia et al., 2017). We found preserved excitable axonal domains at 5 weeks, AIS shortening at 10 and 26 weeks of age and nodal elongation at 26 weeks of age (Specific Aim 2). *Db/db* mice die prematurely at around 10 months of age.

REFERENCES

Arancibia-Carcamo IL, Attwell D (2014) The node of Ranvier in CNS pathology. Acta Neuropathol 128:161–175. doi:10.1007/s00401-014-1305-z.

Athanasiu L et al. (2010) Gene variants associated with schizophrenia in a Norwegian genome-wide study are replicated in a large European cohort. J Psychiatr Res 44:748–753. doi:10.1016/j.jpsychires.2010.02.002.

Baalman KL, Cotton RJ, Rasband SN, Rasband MN (2013) Blast Wave Exposure Impairs Memory and Decreases Axon Initial Segment Length. J Neurotrauma 30:741–751. doi:10.1089/neu.2012.2478.

Babbs CF, Shi R (2013) Subtle Paranodal Injury Slows Impulse Conduction in a Mathematical Model of Myelinated Axons Hamblin M, ed. PLoS One 8:e67767. doi:10.1371/journal.pone.0067767.

Bélanger A, Lavoie N, Trudeau F, Massicotte G, Gagnon S (2004) Preserved LTP and water maze learning in hyperglycaemic-hyperinsulinemic ZDF rats. Physiol Behav 83:483–494. doi:10.1016/j.physbeh.2004.08.031.

Bender KJ, Trussell LO (2012) The Physiology of the Axon Initial Segment. Annu Rev Neurosci 35:249–265. doi:10.1146/annurev-neuro-062111-150339.

Benned-Jensen T, Christensen RK, Denti F, Perrier J-F, Rasmussen HB, Olesen S-P (2016) Live Imaging of Kv7.2/7.3 Cell Surface Dynamics at the Axon Initial Segment: High Steady-State Stability and Calpain-Dependent Excitotoxic Downregulation Revealed. J Neurosci 36:2261–2266. doi:10.1523/JNEUROSCI.2631-15.2016.

Berger SL, Leo-Macias A, Yuen S, Khatri L, Pfennig S, Zhang Y, Agullo-Pascual E, Caillol G, Zhu M-S, Rothenberg E, Melendez-Vasquez C V, Delmar M, Leterrier C, Salzer JL (2018) Localized Myosin II Activity Regulates Assembly and Plasticity of the Axon Initial Segment. Neuron 97:555-570.e6. doi:10.1016/j.neuron.2017.12.039.

Bhat MA, Rios JC, Lu Y, Garcia-Fresco GP, Ching W, St Martin M, Li J, Einheber S, Chesler M, Rosenbluth J, Salzer JL, Bellen HJ (2001) Axon-glia interactions and the domain organization of myelinated axons requires neurexin IV/Caspr/Paranodin. Neuron 30:369–383.

Bierhaus A et al. (2012) Methylglyoxal modification of Na v 1.8 facilitates nociceptive neuron firing and causes hyperalgesia in diabetic neuropathy. Nat Med 18:926–933. doi:10.1038/nm.2750.

Biessels GJ, Kamal A, Ramakers GM, Urban IJ, Spruijt BM, Erkelens DW, Gispen WH (1996) Place learning and hippocampal synaptic plasticity in streptozotocin-induced diabetic rats. Diabetes 45:1259–1266.

Biessels GJ, Strachan MWJ, Visseren FLJ, Kappelle LJ, Whitmer RA (2014) Dementia and cognitive decline in type 2 diabetes and prediabetic stages: Towards targeted interventions. Lancet Diabetes Endocrinol 2:246–255. doi:10.1016/S2213-8587(13)70088-3.

Black S, Kraemer K, Shah A, Simpson G, Scogin F, Smith A (2018) Diabetes, Depression, and Cognition: a Recursive Cycle of Cognitive Dysfunction and Glycemic Dysregulation. Curr Diab Rep 18:118. doi:10.1007/s11892-018-1079-0.

Boström P, Wu J, Jedrychowski MP, Korde A, Ye L, Lo JC, Rasbach KA, Boström EA, Choi JH, Long JZ, Kajimura S, Zingaretti MC, Vind BF, Tu H, Cinti S, Højlund K, Gygi SP, Spiegelman BM (2012) A PGC1-α-dependent myokine that drives brown-fat-like development of white fat and thermogenesis. Nature 481:463–468. doi:10.1038/nature10777.

Boyle ME, Berglund EO, Murai KK, Weber L, Peles E, Ranscht B (2001) Contactin orchestrates assembly of the septate-like junctions at the paranode in myelinated peripheral nerve. Neuron 30:385–397.

Bracke A, Domanska G, Bracke K, Harzsch S, Brandt J van den (2019) Obesity alters mobility and adult neurogenesis , but not hippocampal dependent learning in ob / ob mice. bioRxiv:537720. doi:10.1101/537720.

Bréchet A, Fache M-P, Brachet A, Ferracci G, Baude A, Irondelle M, Pereira S, Leterrier C, Dargent B (2008) Protein kinase CK2 contributes to the organization of sodium channels in axonal membranes by regulating their interactions with ankyrin G. J Cell Biol 183:1101–1114. doi:10.1083/jcb.200805169.

Buettner R, Parhofer KG, Woenckhaus M, Wrede CE, Kunz-Schughart LA, Schölmerich J, Bollheimer LC (2006) Defining high-fat-diet rat models: Metabolic and molecular effects of different fat types. J Mol Endocrinol 36:485–501. doi:10.1677/jme.1.01909.

Castillo-Gómez E, Coviello S, Perez-Rando M, Curto Y, Carceller H, Salvador A, Nacher J (2015) Streptozotocin diabetic mice display depressive-like behavior and alterations in the structure, neurotransmission and plasticity of medial prefrontal cortex interneurons. Brain Res Bull 116:45–56. doi:10.1016/j.brainresbull.2015.06.002.

Chand AN, Galliano E, Chesters RA, Grubb MS (2015) A distinct subtype of dopaminergic interneuron displays inverted structural plasticity at the axon initial segment. J Neurosci 35:1573–1590. doi:10.1523/JNEUROSCI.3515-14.2015.

Chen H, Charlat O, Tartaglia LA, Woolf EA, Weng X, Ellis SJ, Lakey ND, Culpepper J, More KJ, Breitbart RE, Duyk GM, Tepper RI, Morgenstern JP (1996) Evidence that the diabetes gene encodes the leptin receptor: Identification of a mutation in the leptin receptor gene in db/db mice. Cell 84:491–495. doi:10.1016/S0092-

8674(00)81294-5.

Chen J, Liang L, Zhan L, Zhou Y, Zheng L, Sun X, Gong J, Sui H, Jiang R, Zhang F, Zhang L (2014a) ZiBuPiYin recipe protects db/db mice from diabetes-associated cognitive decline through improving multiple pathological changes Cai H, ed. PLoS One 9:e91680. doi:10.1371/journal.pone.0091680.

Chen Y, Liu Z, Zhang J, Xu K, Zhang S, Wei D, Zhang Z (2014b) Altered brain activation patterns under different working memory loads in patients with type 2 diabetes. Diabetes Care 37:3157–3163. doi:10.2337/dc14-1683.

Chornenkyy Y, Wang WX, Wei A, Nelson PT (2018) Alzheimer's disease and Type 2 Diabetes mellitus are distinct diseases with potential overlapping metabolic dysfunction upstream of observed cognitive decline. Brain Pathol 29:3–17. doi:10.1111/bpa.12655.

Clark KC, Josephson A, Benusa SD, Hartley RK, Baer M, Thummala S, Joslyn M, Sword BA, Elford H, Oh U, Dilsizoglu-Senol A, Lubetzki C, Davenne M, DeVries GH, Dupree JL (2016a) Compromised axon initial segment integrity in EAE is preceded by microglial reactivity and contact. Glia 64:1190–1209. doi:10.1002/glia.22991.

Clark KC, Josephson A, Benusa SD, Hartley RK, Baer M, Thummala S, Joslyn M, Sword BA, Elford H, Oh U, Dilsizoglu-Senol A, Lubetzki C, Davenne M, DeVries GH, Dupree JL (2016b) Compromised axon initial segment integrity in EAE is preceded by microglial reactivity and contact. Glia 64:1190–1209. doi:10.1002/glia.22991.

Clark KC, Sword BA, Dupree JL (2017) Oxidative Stress Induces Disruption of the Axon Initial Segment. ASN Neuro 9:1759091417745426. doi:10.1177/1759091417745426.

Coban H, Tung S, Yoo B, Vinters H V, Hinman JD (2017) Molecular disorganization of axons adjacent to human cortical microinfarcts. Front Neurol 8:405. doi:10.1007/s00424-009-0722-7.

Coleman DL, Hummel KP (1974) Hyperinsulinemia in pre-weaning diabetes (db) mice. Diabetologia 10 Suppl:607–610.

Coman I, Aigrot MS, Seilhean D, Reynolds R, Girault JA, Zalc B, Lubetzki C (2006) Nodal, paranodal and juxtaparanodal axonal proteins during demyelination and remyelination in multiple sclerosis. Brain 129:3186–3195. doi:10.1093/brain/awl144.

Cooper MA, Ryals JM, Wu P-Y, Wright KD, Walter KR, Wright DE (2017) Modulation of diet-induced mechanical allodynia by metabolic parameters and inflammation. J Peripher Nerv Syst 22:39–46. doi:10.1111/jns.12199.

Cruz DA, Weaver CL, Lovallo EM, Melchitzky DS, Lewis DA (2009) Selective alterations in postsynaptic markers of chandelier cell inputs to cortical pyramidal neurons in subjects with schizophrenia. Neuropsychopharmacology 34:2112–2124.

doi:10.1038/npp.2009.36.

Cui Y, Jin J, Zhang X, Xu H, Yang L, Du D, Zeng Q, Tsien JZ, Yu H, Cao X (2011) Forebrain NR2B overexpression facilitating the prefrontal cortex long-term potentiation and enhancing working memory function in mice. PLoS One 6:e20312. doi:10.1371/journal.pone.0020312.

del Puerto A, Fronzaroli-Molinieres L, Perez-Alvarez MJ, Giraud P, Carlier E, Wandosell F, Debanne D, Garrido JJ (2015) ATP-P2X7 Receptor Modulates Axon Initial Segment Composition and Function in Physiological Conditions and Brain Injury. Cereb Cortex 25:2282–2294. doi:10.1093/cercor/bhu035.

Dhar M, Zhu M, Impey S, Lambert TJ, Bland T, Karatsoreos IN, Nakazawa T, Appleyard SM, Wayman GA (2014) Leptin Induces Hippocampal Synaptogenesis via CREB-Regulated MicroRNA-132 Suppression of p250GAP. Mol Endocrinol 28:1073–1087. doi:10.1210/me.2013-1332.

Dinel A-L, André C, Aubert A, Ferreira G, Layé S, Castanon N (2011) Cognitive and emotional alterations are related to hippocampal inflammation in a mouse model of metabolic syndrome. Block ML, ed. PLoS One 6:e24325. doi:10.1371/journal.pone.0024325.

Erickson JR, Pereira L, Wang L, Han G, Ferguson A, Dao K, Copeland RJ, Despa F, Hart GW, Ripplinger CM, Bers DM (2013) Diabetic hyperglycaemia activates CaMKII and arrhythmias by O-linked glycosylation. Nature 502:372–376. doi:10.1038/nature12537.

Ernst A, Sharma AN, Elased KM, Guest PC, Rahmoune H, Bahn S (2013) Diabetic db/db mice exhibit central nervous system and peripheral molecular alterations as seen in neurological disorders. Transl Psychiatry 3:e263. doi:10.1038/tp.2013.42.

Evans MD, Dumitrescu AS, Kruijssen DLH, Taylor SE, Grubb MS (2015) Rapid Modulation of Axon Initial Segment Length Influences Repetitive Spike Firing. Cell Rep 13:1233–1245. doi:10.1016/j.celrep.2015.09.066.

Evans MD, Sammons RP, Lebron S, Dumitrescu AS, Watkins TBK, Uebele VN, Renger JJ, Grubb MS (2013) Calcineurin Signaling Mediates Activity-Dependent Relocation of the Axon Initial Segment. J Neurosci 33:6950–6963. doi:10.1523/JNEUROSCI.0277-13.2013.

Evans MD, Tufo C, Dumitrescu AS, Grubb MS (2017) Myosin II activity is required for structural plasticity at the axon initial segment. Eur J Neurosci 46:1751–1757. doi:10.1111/ejn.13597.

Feil DG, Zhu CW, Sultzer DL (2012) The relationship between cognitive impairment and diabetes self-management in a population-based community sample of older adults with Type 2 diabetes. J Behav Med 35:190–199. doi:10.1007/s10865-011-9344-6.

Franssen H, Straver DCG (2013) Pathophysiology of immune-mediated demyelinating neuropathies-part I: Neuroscience. Muscle Nerve 48:851–864. doi:10.1002/mus.24070.

Fruhwürth S, Vogel H, Schürmann A, Williams KJ (2018) Novel insights into how overnutrition disrupts the hypothalamic actions of leptin. Front Endocrinol (Lausanne) 9:89. doi:10.3389/fendo.2018.00089.

Fu Z, Wu J, Nesil T, Li MD, Aylor KW, Liu Z (2017) Long-term high-fat diet induces hippocampal microvascular insulin resistance and cognitive dysfunction. Am J Physiol - Endocrinol Metab 312:E89–E97. doi:10.1152/ajpendo.00297.2016.

Giesbertz P, Padberg I, Rein D, Ecker J, Höfle AS, Spanier B, Daniel H (2015) Metabolite profiling in plasma and tissues of ob/ob and db/db mice identifies novel markers of obesity and type 2 diabetes. Diabetologia 58:2133–2143. doi:10.1007/s00125-015-3656-y.

Gold SM, Dziobek I, Sweat V, Tirsi A, Rogers K, Bruehl H, Tsui W, Richardson S, Javier E, Convit A (2007) Hippocampal damage and memory impairments as possible early brain complications of type 2 diabetes. Diabetologia 50:711–719. doi:10.1007/s00125-007-0602-7.

Greer JE, Hånell A, McGinn MJ, Povlishock JT (2013) Mild traumatic brain injury in the mouse induces axotomy primarily within the axon initial segment. Acta Neuropathol 126:59–74. doi:10.1007/s00401-013-1119-4.

Griggs RB, Yermakov LM, Drouet DE, Nguyen DVM, Susuki K (2018) Methylglyoxal Disrupts Paranodal Axoglial Junctions via Calpain Activation. ASN Neuro 10:175909141876617. doi:10.1177/1759091418766175.

Griggs RB, Yermakov LM, Susuki K (2017) Formation and disruption of functional domains in myelinated CNS axons. Neurosci Res 116:77–87. doi:10.1016/j.neures.2016.09.010.

Gu C, Zhou W, Wang W, Xiang H, Xu H, Liang L, Sui H, Zhan L, Lu X (2017) ZiBuPiYin recipe improves cognitive decline by regulating gut microbiota in Zucker diabetic fatty rats. Oncotarget 8:27693–27703. doi:10.18632/oncotarget.14611.

Guimarães J, Sá MJ (2012) Cognitive Dysfunction in Multiple Sclerosis. Front Neurol 3:74. doi:10.3389/fneur.2012.00074.

Guo M, Lu XY (2014) Leptin receptor deficiency confers resistance to behavioral effects of fluoxetine and desipramine via separable substrates. Transl Psychiatry 4:e486. doi:10.1038/tp.2014.126.

Guo Y, Su Z-J, Chen Y-K, Chai Z (2017) Brain-derived neurotrophic factor/neurotrophin 3 regulate axon initial segment location and affect neuronal excitability in cultured hippocampal neurons. J Neurochem 142:260–271. doi:10.1111/jnc.14050.

Gutzmann A, Ergül N, Grossmann R, Schultz C, Wahle P, Engelhardt M (2014) A period of structural plasticity at the axon initial segment in developing visual cortex. Front Neuroanat 8:11. doi:10.3389/fnana.2014.00011.

Hamada MS, Kole MHP (2015) Myelin loss and axonal ion channel adaptations associated with gray matter neuronal hyperexcitability. J Neurosci 35:7272–7286. doi:10.1523/JNEUROSCI.4747-14.2015.

Harty RC, Kim TH, Thomas EA, Cardamone L, Jones NC, Petrou S, Wimmer VC (2013) Axon initial segment structural plasticity in animal models of genetic and acquired epilepsy. Epilepsy Res 105:272–279. doi:10.1016/j.eplepsyres.2013.03.004.

Hatch RJ, Wei Y, Xia D, Götz J (2017) Hyperphosphorylated tau causes reduced hippocampal CA1 excitability by relocating the axon initial segment. Acta Neuropathol 133:717–730. doi:10.1007/s00401-017-1674-1.

Hendry SH, Schwark HD, Jones EG, Yan J (1987) Numbers and proportions of GABA-immunoreactive neurons in different areas of monkey cerebral cortex. J Neurosci 7:1503–1519.

Hien YE, Montersino A, Castets F, Leterrier C, Filhol O, Vacher H, Dargent B (2014) CK2 accumulation at the axon initial segment depends on sodium channel Nav1. FEBS Lett 588:3403–3408. doi:10.1016/j.febslet.2014.07.032.

Hinman JD, Lee MD, Tung S, Vinters H V., Carmichael ST (2015) Molecular disorganization of axons adjacent to human lacunar infarcts. Brain 138:736–745. doi:10.1093/brain/awu398.

Hinman JD, Peters A, Cabral H, Rosene DL, Hollander W, Rasband MN, Abraham CR (2006) Age-related molecular reorganization at the node of Ranvier. J Comp Neurol 495:351–362. doi:10.1002/cne.20886.

Hinman JD, Rasband MN, Carmichael ST (2013) Remodeling of the axon initial segment after focal cortical and white matter stroke. Stroke 44:182–189. doi:10.1161/STROKEAHA.112.668749.

Höfflin F, Jack A, Riedel C, Mack-Bucher J, Roos J, Corcelli C, Schultz C, Wahle P, Engelhardt M (2017) Heterogeneity of the Axon Initial Segment in Interneurons and Pyramidal Cells of Rodent Visual Cortex. Front Cell Neurosci 11:332. doi:10.3389/fncel.2017.00332.

Howell OW, Palser A, Polito A, Melrose S, Zonta B, Scheiermann C, Vora AJ, Brophy PJ, Reynolds R (2006) Disruption of neurofascin localization reveals early changes preceding demyelination and remyelination in multiple sclerosis. Brain 129:3173–3185. doi:10.1093/brain/awl290.

Hsu JL, Chen YL, Leu JG, Jaw FS, Lee CH, Tsai YF, Hsu CY, Bai CH, Leemans A (2012) Microstructural white matter abnormalities in type 2 diabetes mellitus: A diffusion tensor imaging study. Neuroimage 59:1098–1105. doi:10.1016/j.neuroimage.2011.09.041.

Huang CY-M, Rasband MN (2018) Axon initial segments: structure, function, and disease. Ann N Y Acad Sci 1420:46–61. doi:10.1111/nyas.13718.

Huang CY-M, Zhang C, Zollinger DR, Leterrier C, Rasband MN (2017) An αII Spectrin-Based Cytoskeleton Protects Large-Diameter Myelinated Axons from Degeneration. J Neurosci 37:11323–11334. doi:10.1523/JNEUROSCI.2113-17.2017.

Hummel KP, Dickie MM, Coleman DL (1966) Diabetes, a new mutation in the mouse. Science 153:1127–1128. doi:10.1126/science.153.3740.1127.

Hund TJ, Koval OM, Li J, Wright PJ, Qian L, Snyder JS, Gudmundsson H, Kline CF, Davidson NP, Cardona N, Rasband MN, Anderson ME, Mohler PJ (2010) A βIV-spectrin/CaMKII signaling complex is essential for membrane excitability in mice. J Clin Invest 120:3508–3519. doi:10.1172/JCI43621.

Hyde LA, Hoplight BJ, Denenberg VH (1998) Water version of the radial-arm maze: Learning in three inbred strains of mice. Brain Res 785:236–244. doi:10.1016/S0006-8993(97)01417-0.

Infante-Garcia C, Jose Ramos-Rodriguez J, Marin-Zambrana Y, Teresa Fernandez-Ponce M, Casas L, Mantell C, Garcia-Alloza M (2017) Mango leaf extract improves central pathology and cognitive impairment in a type 2 diabetes mouse model. Brain Pathol 27:499–507. doi:10.1111/bpa.12433.

Jacko M, Weyn-Vanhentenryck SM, Smerdon JW, Yan R, Feng H, Williams DJ, Pai J, Xu K, Wichterle H, Zhang C (2018) Rbfox Splicing Factors Promote Neuronal Maturation and Axon Initial Segment Assembly. Neuron 97:853-868.e6. doi:10.1016/j.neuron.2018.01.020.

Jamann N, Jordan M, Engelhardt M (2018) Activity-dependent axonal plasticity in sensory systems. Neuroscience 368:268–282. doi:10.1016/j.neuroscience.2017.07.035.

Knowler WC, Barrett-Connor E, Fowler SE, Hamman RF, Lachin JM, Walker EA, Nathan DM, Diabetes Prevention Program Research Group (2002) Reduction in the Incidence of Type 2 Diabetes with Lifestyle Intervention or Metformin. N Engl J Med 346:393–403. doi:10.1056/NEJMoa012512.

Kole MHP, Stuart GJ (2012) Signal Processing in the Axon Initial Segment. Neuron 73:235–247. doi:10.1016/j.neuron.2012.01.007.

Kuba H, Oichi Y, Ohmori H (2010) Presynaptic activity regulates Na+ channel distribution at the axon initial segment. Nature 465:1075–1078. doi:10.1038/nature09087.

Kumar A, Haroon E, Darwin C, Pham D, Ajilore O, Rodriguez G, Mintz J (2008) Gray matter prefrontal changes in type 2 diabetes detected using MRI. J Magn Reson Imaging 27:14–19. doi:10.1002/jmri.21224.

Larsson M, Lietzau G, Nathanson D, Ostenson C-G, Mallard C, Johansson ME, Nystrom T, Patrone C, Darsalia V (2016) Diabetes negatively affects cortical and striatal GABAergic neurons: an effect that is partially counteracted by exendin-4. Biosci Rep 36:e00421–e00421. doi:10.1042/bsr20160437.

Leinninger GM, Myers MG (2007) LRb signals act within a distributed network of leptin-responsive neurones to mediate leptin action. Acta Physiol 192:49–59. doi:10.1111/j.1748-1716.2007.01784.x.

Lezmy J, Lipinsky M, Khrapunsky Y, Patrich E, Shalom L, Peretz A, Fleidervish IA, Attali B (2017) M-current inhibition rapidly induces a unique CK2-dependent plasticity of the axon initial segment. Proc Natl Acad Sci U S A 114:E10234–

E10243. doi:10.1073/pnas.1708700114.

Li XL, Aou S, Oomura Y, Hori N, Fukunaga K, Hori T (2002) Impairment of long-term potentiation and spatial memory in leptin receptor-deficient rodents. Neuroscience 113:607–615. doi:10.1016/S0306-4522(02)00162-8.

Manschot SM, Brands AMA, Van Der Grond J, Kessels RPC, Algra A, Kappelle LJ, Biessels GJ (2006) Brain magnetic resonance imaging correlates of impaired cognition in patients with type 2 diabetes. Diabetes 55:1106–1113. doi:10.2337/diabetes.55.04.06.db05-1323.

Marella M, Patki G, Matsuno-Yagi A, Yagi T (2013) Complex I inhibition in the visual pathway induces disorganization of the node of Ranvier. Neurobiol Dis 58:281–288. doi:10.1016/j.nbd.2013.06.010.

Marin MA, Ziburkus J, Jankowsky J, Rasband MN (2016) Amyloid-β plaques disrupt axon initial segments. Exp Neurol 281:93–98. doi:10.1016/j.expneurol.2016.04.018.

Miyake A, Friedman NP, Emerson MJ, Witzki AH, Howerter A, Wager TD (2000) The Unity and Diversity of Executive Functions and Their Contributions to Complex "Frontal Lobe" Tasks: A Latent Variable Analysis. Cogn Psychol 41:49–100. doi:10.1006/cogp.1999.0734.

Miyata S, Taniguchi M, Koyama Y, Shimizu S, Tanaka T, Yasuno F, Yamamoto A, Iida H, Kudo T, Katayama T, Tohyama M (2016) Association between chronic stress-induced structural abnormalities in Ranvier nodes and reduced oligodendrocyte activity in major depression. Sci Rep 6:23084. doi:10.1038/srep23084.

Nam SM, Yoo DY, Kwon HJ, Kim JW, Jung HY, Kim DW, Han HJ, Won M-H, Seong JK, Hwang IK, Yoon YS (2017) Proteomic approach to detect changes in hippocampal protein levels in an animal model of type 2 diabetes. Neurochem Int 108:246–253. doi:10.1016/j.neuint.2017.04.011.

Nelson AD, Caballero-Florán RN, Rodríguez Díaz JC, Hull JM, Yuan Y, Li J, Chen K, Walder KK, Lopez-Santiago LF, Bennett V, McInnis MG, Isom LL, Wang C, Zhang M, Jones KS, Jenkins PM (2018) Ankyrin-G regulates forebrain connectivity and network synchronization via interaction with GABARAP. Mol Psychiatry. doi:10.1038/s41380-018-0308-x.

Nelson AD, Jenkins PM (2017) Axonal Membranes and Their Domains: Assembly and Function of the Axon Initial Segment and Node of Ranvier. Front Cell Neurosci 11:136. doi:10.3389/fncel.2017.00136.

Neth BJ, Craft S (2017) Insulin resistance and Alzheimer's disease: Bioenergetic linkages. Front Aging Neurosci 9:345. doi:10.3389/fnagi.2017.00345.

Palta P, Schneider ALC, Biessels GJ, Touradji P, Hill-Briggs F (2014) Magnitude of cognitive dysfunction in adults with type 2 diabetes: A meta-analysis of six cognitive domains and the most frequently reported neuropsychological tests within domains. J Int Neuropsychol Soc 20:278–291. doi:10.1017/S1355617713001483.

Pan XR, Li GW, Hu YH, Wang JX, Yang WY, An ZX, Hu ZX, Lin J, Xiao JZ, Cao HB,

Liu PA, Jiang XG, Jiang YY, Wang JP, Zheng H, Zhang H, Bennett PH, Howard B V (1997) Effects of diet and exercise in preventing NIDDM in people with impaired glucose tolerance. The Da Qing IGT and Diabetes Study. Diabetes Care 20:537–544.

Pan Z, Kao T, Horvath Z, Lemos J, Sul J-Y, Cranstoun SD, Bennett V, Scherer SS, Cooper EC (2006) A common ankyrin-G-based mechanism retains KCNQ and NaV channels at electrically active domains of the axon. J Neurosci 26:2599–2613. doi:10.1523/JNEUROSCI.4314-05.2006.

Peles E, Nativ M, Lustig M, Grumet M, Schilling J, Martinez R, Plowman GD, Schlessinger J (1997) Identification of a novel contactin-associated transmembrane receptor with multiple domains implicated in protein-protein interactions. EMBO J 16:978–988. doi:10.1093/emboj/16.5.978.

Peterson RG, Shaw WN, Neel M-A, Little LA, Eichberg J (1990) Zucker Diabetic Fatty Rat as a Model for Non-insulin-dependent Diabetes Mellitus. ILAR J 32:16–19. doi:10.1093/ilar.32.3.16.

Pu D, Zhao Y, Chen J, Sun Y, Lv A, Zhu S, Luo C, Zhao K, Xiao Q (2018) Protective Effects of Sulforaphane on Cognitive Impairments and AD-like Lesions in Diabetic Mice are Associated with the Upregulation of Nrf2 Transcription Activity. Neuroscience 381:35–45. doi:10.1016/j.neuroscience.2018.04.017.

Radecki DZ, Johnson EL, Brown AK, Meshkin NT, Perrine SA, Gow A (2018) Corticohippocampal Dysfunction In The OBiden Mouse Model Of Primary Oligodendrogliopathy. Sci Rep 8:16116. doi:10.1038/s41598-018-34414-7.

Ramos-Rodriguez JJ, Ortiz O, Jimenez-Palomares M, Kay KR, Berrocoso E, Murillo-Carretero MI, Perdomo G, Spires-Jones T, Cozar-Castellano I, Lechuga-Sancho AM, Garcia-Alloza M (2013) Differential central pathology and cognitive impairment in pre-diabetic and diabetic mice. Psychoneuroendocrinology 38:2462–2475. doi:10.1016/j.psyneuen.2013.05.010.

Rasband MN, Peles E (2016) The nodes of Ranvier: Molecular assembly and maintenance. Cold Spring Harb Perspect Biol 8:a020495. doi:10.1101/cshperspect.a020495.

Rosenbluth J (2009) Multiple functions of the paranodal junction of myelinated nerve fibers. J Neurosci Res 87:3250–3258. doi:10.1002/jnr.22013.

Roussos P, Haroutunian V (2014) Schizophrenia: susceptibility genes and oligodendroglial and myelin related abnormalities. Front Cell Neurosci 8:5. doi:10.3389/fncel.2014.00005.

Roussos P, Katsel P, Davis KL, Bitsios P, Giakoumaki SG, Jogia J, Rozsnyai K, Collier D, Frangou S, Siever LJ, Haroutunian V (2012) Molecular and genetic evidence for abnormalities in the nodes of Ranvier in schizophrenia. Arch Gen Psychiatry 69:7–15. doi:10.1001/archgenpsychiatry.2011.110.

Sadanand S, Balachandar R, Bharath S (2016) Memory and executive functions in

persons with type 2 diabetes: A meta-analysis. Diabetes Metab Res Rev 32:132–142. doi:10.1002/dmrr.2664.

Sahara S, Yanagawa Y, O'Leary DDM, Stevens CF (2012) The fraction of cortical GABAergic neurons is constant from near the start of cortical neurogenesis to adulthood. J Neurosci 32:4755–4761. doi:10.1523/JNEUROSCI.6412-11.2012.

Satake T, Yamashita K, Hayashi K, Miyatake S, Tamura-Nakano M, Doi H, Furuta Y, Shioi G, Miura E, Takeo YH, Yoshida K, Yahikozawa H, Matsumoto N, Yuzaki M, Suzuki A (2017) MTCL1 plays an essential role in maintaining Purkinje neuron axon initial segment. EMBO J 36:1227–1242. doi:10.15252/embj.201695630.

Schafer DP, Jha S, Liu F, Akella T, McCullough LD, Rasband MN (2009) Disruption of the axon initial segment cytoskeleton is a new mechanism for neuronal injury. J Neurosci 29:13242–13254. doi:10.1523/JNEUROSCI.3376-09.2009.

Schindelin J, Arganda-Carreras I, Frise E, Kaynig V, Longair M, Pietzsch T, Preibisch S, Rueden C, Saalfeld S, Schmid B, Tinevez JY, White DJ, Hartenstein V, Eliceiri K, Tomancak P, Cardona A (2012) Fiji: An open-source platform for biological-image analysis. Nat Methods 9:676–682. doi:10.1038/nmeth.2019.

Semenkovich K, Bischoff A, Doty T, Nelson S, Siller AF, Hershey T, Arbeláez AM (2016a) Clinical presentation and memory function in youth with type 1 diabetes. Pediatr Diabetes 17:492–499. doi:10.1111/pedi.12314.

Semenkovich K, Patel PP, Pollock AB, Beach KA, Nelson S, Masterson JJ, Hershey T, Arbeláez AM (2016b) Academic abilities and glycaemic control in children and young people with Type 1 diabetes mellitus. Diabet Med 33:668–673. doi:10.1111/dme.12854.

Sharma AN, Elased KM, Garrett TL, Lucot JB (2010) Neurobehavioral deficits in db/db diabetic mice. Physiol Behav 101:381–388. doi:10.1016/j.physbeh.2010.07.002.

Sharma AN, Elased KM, Lucot JB (2012) Rosiglitazone treatment reversed depression- but not psychosis-like behavior of db/db diabetic mice. J Psychopharmacol 26:724–732. doi:10.1177/0269881111434620.

Shiers S, Pradhan G, Mwirigi J, Mejia G, Ahmad A, Kroener S, Price T (2018) Neuropathic Pain Creates an Enduring Prefrontal Cortex Dysfunction Corrected by the Type II Diabetic Drug Metformin But Not by Gabapentin. J Neurosci 38:7337–7350. doi:10.1080/00288233.1960.10418075.

Sigal RJ, Kenny GP, Wasserman DH, Castaneda-Sceppa C, White RD (2006) Physical activity/exercise and type 2 diabetes: a consensus statement from the American Diabetes Association. Diabetes Care 29:1433–1438. doi:10.2337/dc06-9910.

Somineni HK, Boivin GP, Elased KM (2014) Daily exercise training protects against albuminuria and angiotensin converting enzyme 2 shedding in db/db diabetic mice. J Endocrinol 221:235–251. doi:10.1530/JOE-13-0532.

Stoeckel LE, Arvanitakis Z, Gandy S, Small D, Kahn CR, Pascual-Leone A, Pawlyk A, Sherwin R, Smith P (2016) Complex mechanisms linking neurocognitive

dysfunction to insulin resistance and other metabolic dysfunction. F1000Research 5:353. doi:10.12688/f1000research.8300.2.

Stranahan AM, Arumugam T V, Cutler RG, Lee K, Egan JM, Mattson MP (2008) Diabetes impairs hippocampal function through glucocorticoid-mediated effects on new and mature neurons. Nat Neurosci 11:309–317. doi:10.1038/nn2055.

Stranahan AM, Lee K, Martin B, Maudsley S, Golden E, Cutler RG, Mattson MP (2009) Voluntary exercise and caloric restriction enhance hippocampal dendritic spine density and BDNF levels in diabetic mice. Hippocampus 19:951–961. doi:10.1002/hipo.20577.

Susuki K, Otani Y, Rasband MN (2016) Submembranous cytoskeletons stabilize nodes of Ranvier. Exp Neurol 283:446–451. doi:10.1016/j.expneurol.2015.11.012.

Tapia M, Dominguez A, Zhang W, Del Puerto A, Ciorraga M, Benitez MJ, Guaza C, Garrido JJ (2017) Cannabinoid Receptors Modulate Neuronal Morphology and AnkyrinG Density at the Axon Initial Segment. Front Cell Neurosci 11:5. doi:10.3389/fncel.2017.00005.

Thabit H, Kyaw Tun T, McDermott J, Sreenan S (2012) Executive Function and Diabetes Mellitus - A Stone Left Unturned? Curr Diabetes Rev 8:109–115. doi:10.2174/157339912799424555.

Trunova S, Baek B, Giniger E (2011) Cdk5 regulates the size of an axon initial segment-like compartment in mushroom body neurons of the Drosophila central brain. J Neurosci 31:10451–10462. doi:10.1523/JNEUROSCI.0117-11.2011.

Udagawa J, Hashimoto R, Suzuki H, Hatta T, Sotomaru Y, Hioki K, Kagohashi Y, Nomura T, Minami Y, Otani H (2006) The role of leptin in the development of the cerebral cortex in mouse embryos. Endocrinology 147:647–658. doi:10.1210/en.2005-0791.

van Sloten T, Schram M (2018) Understanding depression in type 2 diabetes: a biological approach in observational studies. F1000Research 7. doi:10.12688/f1000research.13898.1.

Vannucci SJ, Willing LB, Goto S, Alkayed NJ, Brucklacher RM, Wood TL, Towfighi J, Hurn PD, Simpson IA (2001) Experimental stroke in the female diabetic, db/db, mouse. J Cereb Blood Flow Metab 21:52–60. doi:10.1097/00004647-200101000-00007.

Vascak M, Sun J, Baer M, Jacobs KM, Povlishock JT (2017) Mild Traumatic Brain Injury Evokes Pyramidal Neuron Axon Initial Segment Plasticity and Diffuse Presynaptic Inhibitory Terminal Loss. Front Cell Neurosci 11:157. doi:10.3389/fncel.2017.00157.

Verma N, Ly H, Liu M, Chen J, Zhu H, Chow M, Hersh LB, Despa F (2016) Intraneuronal Amylin Deposition, Peroxidative Membrane Injury and Increased IL-1β Synthesis in Brains of Alzheimer's Disease Patients with Type-2 Diabetes and in Diabetic HIP Rats. J Alzheimer's Dis 53:259–272. doi:10.3233/JAD-160047.

Vorhees C V, Williams MT (2006) Morris water maze: Procedures for assessing spatial and related forms of learning and memory. Nat Protoc 1:848–858. doi:10.1038/nprot.2006.116.

Wang B, Chandrasekera PC, Pippin JJ (2014a) Leptin- and leptin receptor-deficient rodent models: relevance for human type 2 diabetes. Curr Diabetes Rev 10:131–145.

Wang H, Chen F, Zhong KL, Tang SS, Hu M, Long Y, Miao MX, Liao JM, Sun HB, Hong H (2016) PPARγ agonists regulate bidirectional transport of amyloid-β across the blood-brain barrier and hippocampus plasticity in *db* / *db* mice. Br J Pharmacol 173:372–385. doi:10.1111/bph.13378.

Wang J-Q, Yin J, Song Y-F, Zhang L, Ren Y-X, Wang D-G, Gao L-P, Jing Y-H (2014b) Brain Aging and AD-Like Pathology in Streptozotocin-Induced Diabetic Rats. J Diabetes Res 2014:1–12. doi:10.1155/2014/796840.

Wang S, Dale GL, Song P, Viollet B, Zou M-H (2010) AMPKalpha1 deletion shortens erythrocyte life span in mice: role of oxidative stress. J Biol Chem 285:19976–19985. doi:10.1074/jbc.M110.102467.

Wrighten SA, Piroli GG, Grillo CA, Reagan LP (2009) A look inside the diabetic brain: Contributors to diabetes-induced brain aging. Biochim Biophys Acta - Mol Basis Dis 1792:444–453. doi:10.1016/j.bbadis.2008.10.013.

Wu Y-J, Lin C-C, Yeh C-M, Chien M-E, Tsao M-C, Tseng P, Huang C-W, Hsu K-S (2017) Repeated transcranial direct current stimulation improves cognitive dysfunction and synaptic plasticity deficit in the prefrontal cortex of streptozotocin-induced diabetic rats. Brain Stimul 10:1079–1087. doi:10.1016/J.BRS.2017.08.007.

Xiang Q, Zhang J, Li C-Y, Wang Y, Zeng M-J, Cai Z-X, Tian R-B, Jia W, Li X-H (2015) Insulin resistance-induced hyperglycemia decreased the activation of Akt/CREB in hippocampus neurons: Molecular evidence for mechanism of diabetes-induced cognitive dysfunction. Neuropeptides 54:9–15. doi:10.1016/j.npep.2015.08.009.

Xu M, Cooper EC (2015) An Ankyrin-G N-terminal Gate and Protein Kinase CK2 Dually Regulate Binding of Voltage-gated Sodium and KCNQ2/3 Potassium Channels. J Biol Chem 290:16619–16632. doi:10.1074/jbc.M115.638932.

Yamada R, Kuba H (2016) Structural and Functional Plasticity at the Axon Initial Segment. Front Cell Neurosci 10:250. doi:10.3389/fncel.2016.00250.

Yoshimura T, Stevens SR, Leterrier C, Stankewich MC, Rasband MN (2016) Developmental Changes in Expression of βIV Spectrin Splice Variants at Axon Initial Segments and Nodes of Ranvier. Front Cell Neurosci 10:304. doi:10.3389/fncel.2016.00304.

Zenker J, Poirot O, de Preux Charles A-S, Arnaud E, Médard J-J, Lacroix C, Kuntzer T, Chrast R (2012) Altered distribution of juxtaparanodal kv1.2 subunits mediates peripheral nerve hyperexcitability in type 2 diabetes mellitus. J Neurosci 32:7493–7498. doi:10.1523/JNEUROSCI.0719-12.2012.

Zhang C, Susuki K, Zollinger DR, Dupree JL, Rasband MN (2013) Membrane domain

organization of myelinated axons requires βII spectrin. J Cell Biol 203:437–443. doi:10.1083/jcb.201308116.

Zhang J, Wang Y, Wang J, Zhou X, Shu N, Wang Y, Zhang Z (2014) White matter integrity disruptions associated with cognitive impairments in type 2 diabetic patients. Diabetes 63:3596–3605. doi:10.2337/db14-0342.

Zhao Q, Matsumoto K, Tsuneyama K, Tanaka K, Li F, Shibahara N, Miyata T, Yokozawa T (2011) Diabetes-induced central cholinergic neuronal loss and cognitive deficit are attenuated by tacrine and a Chinese herbal prescription, Kangen-karyu: Elucidation in type 2 diabetes db/db mice. J Pharmacol Sci 117:230–242. doi:10.1254/jphs.11115FP.

Zheng H, Zheng Y, Zhao L, Chen M, Bai G, Hu Y, Hu W, Yan Z, Gao H (2017) Cognitive decline in type 2 diabetic db/db mice may be associated with brain region-specific metabolic disorders. Biochim Biophys Acta - Mol Basis Dis 1863:266–273. doi:10.1016/J.BBADIS.2016.11.003.

APPENDIX

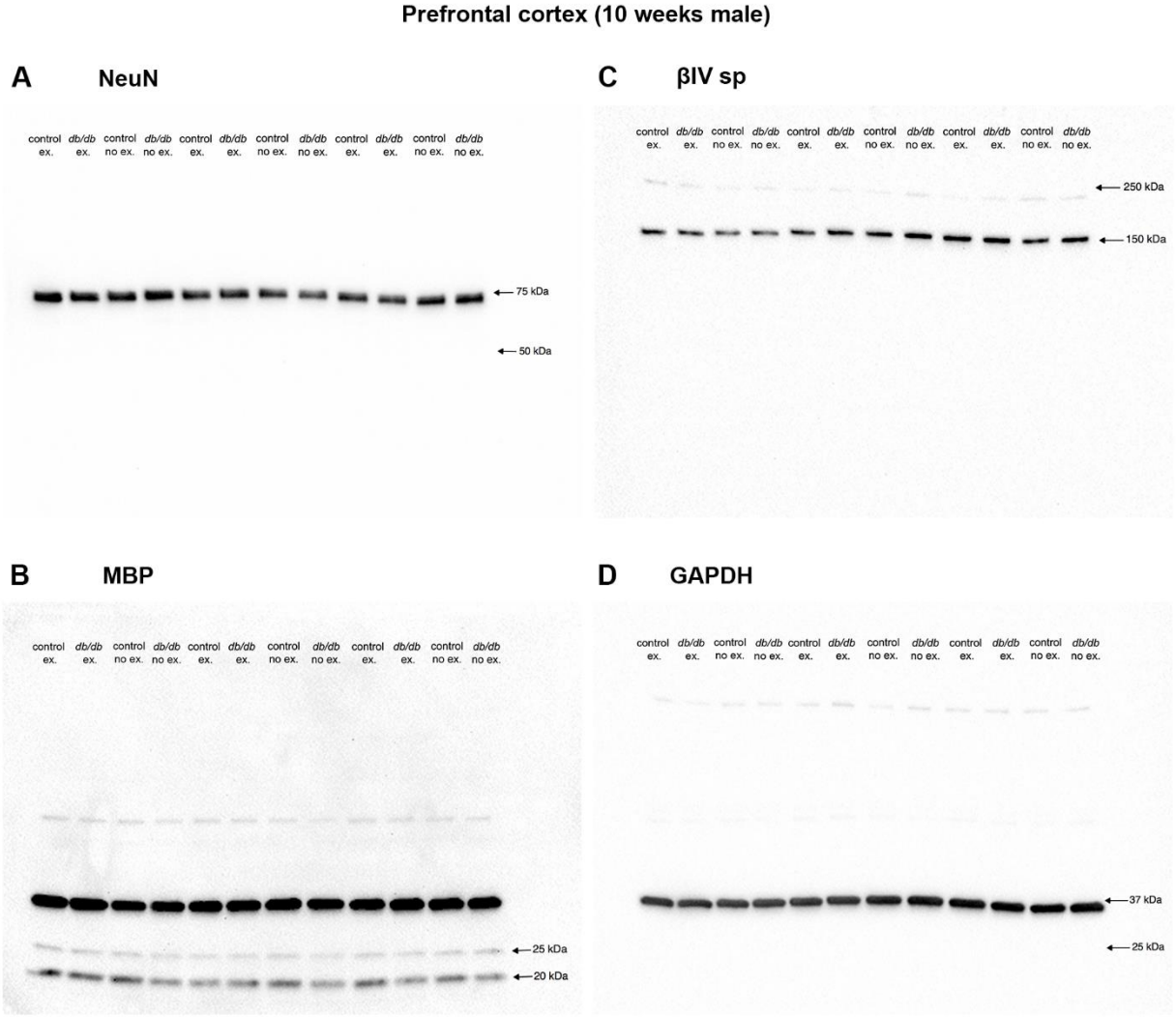

Supplementary Figure S1. Original immunoblots for Figure 3.4B.

Original full-size immunoblots of homogenized frontal brains, stained with antibody to NeuN **(A)**, MBP **(B)**, βIV spectrin **(C)**, and GAPDH **(D)**.

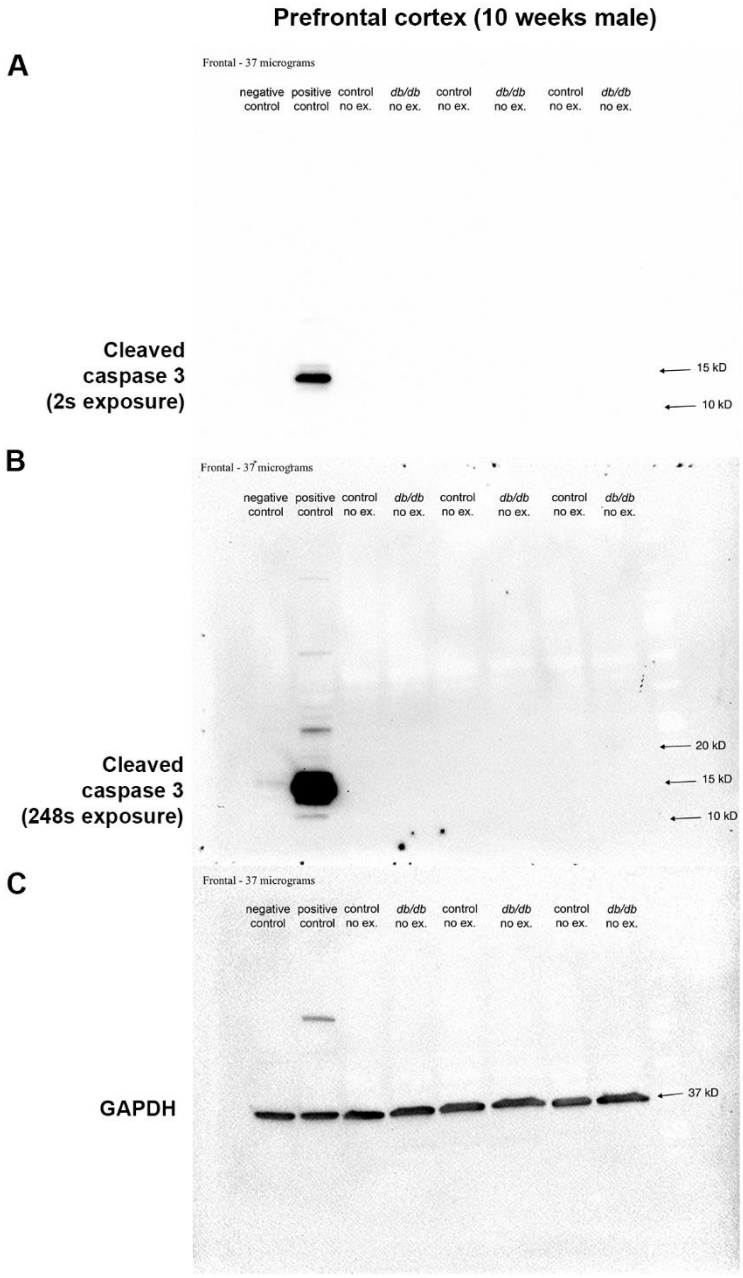

Supplementary Figure S2. Original immunoblots for Figure 3.4D.

(A-C) Original full-size immunoblot of homogenized frontal lobes, stained with antibody to cleaved caspase 3, with short exposure time **(A)** or long exposure time **(B)**; and stained with antibody to GAPDH **(C)**. Untreated Jurkat (negative control) and Jurkat cells + Cytochrome c (positive control) were used as controls (Cell Signaling Technology Cat#9663).

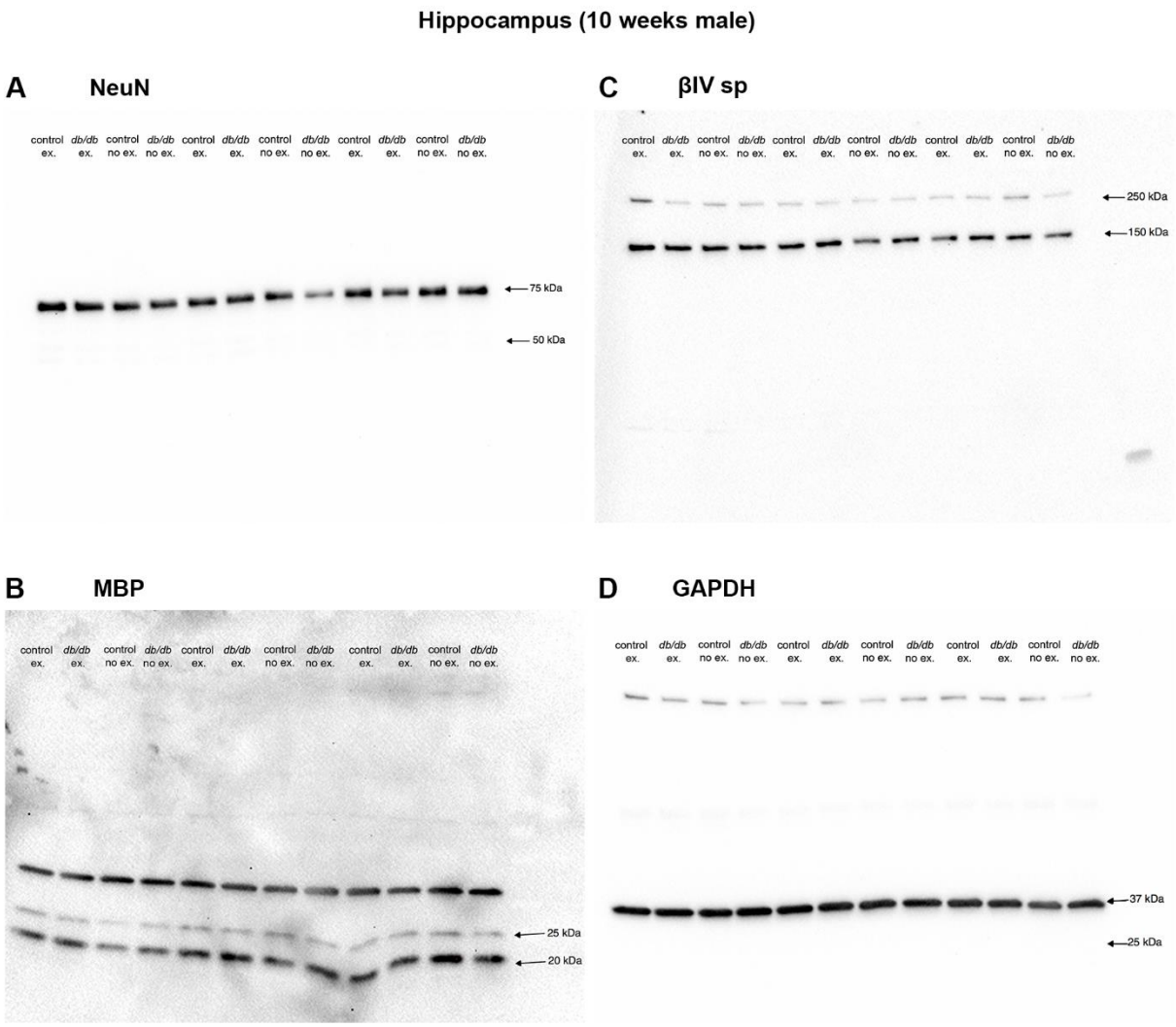

Supplementary Figure S3. Original immunoblots for Figure 3.5B.

Original full-size immunoblots of homogenized hippocampi, stained with antibody to NeuN **(A)**, MBP **(B)**, βIV spectrin **(C)**, and GAPDH **(D)**.

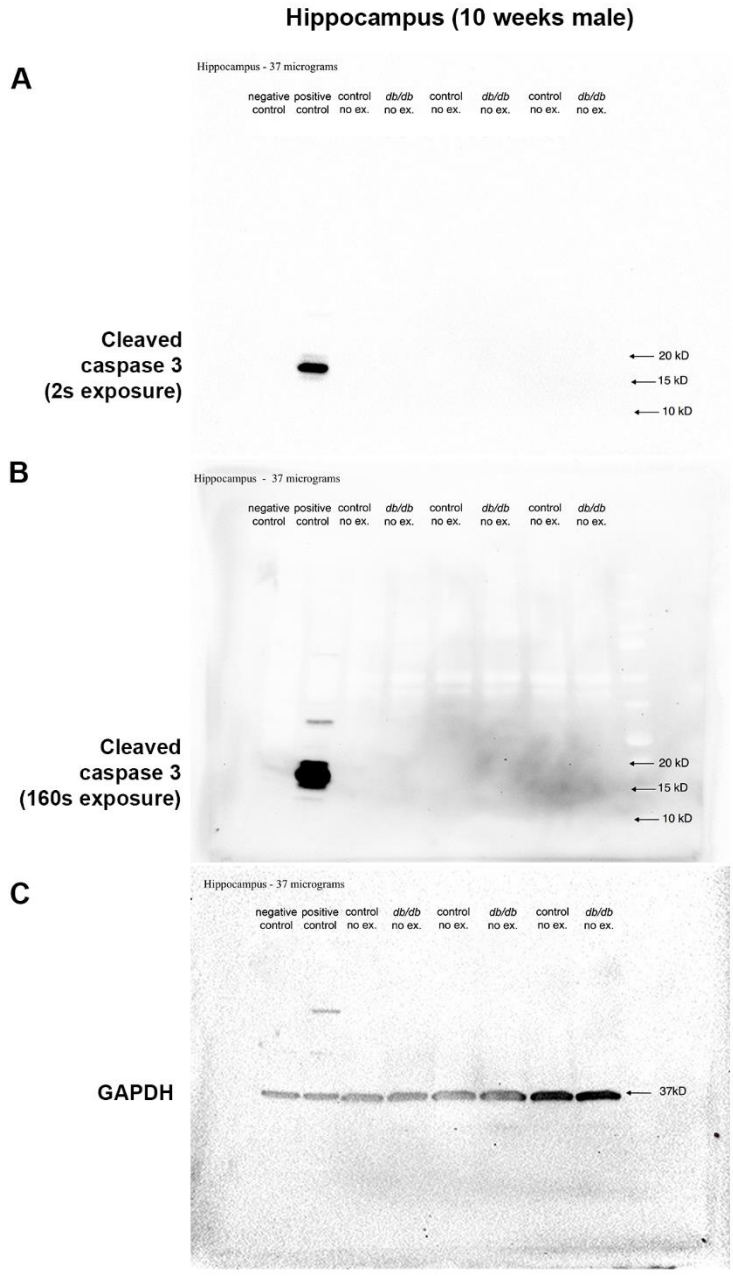

Supplementary Figure S4. Original immunoblots for Figure 3.5D.

(A-C) Original full-size immunoblot of homogenized hippocampi, stained with antibody to cleaved caspase 3, with short exposure time **(A)** or long exposure time **(B)**; and stained with antibody to GAPDH **(C)**. Untreated Jurkat (negative control) and Jurkat cells + Cytochrome c (positive control) were used as controls (Cell Signaling Technology Cat#9663).